

PREPARED FOR SUBMISSION TO JHEP

Seeking leptoquarks in IceCube

Damir Bečirević,^a Boris Panes,^b Olcyr Sumensari^{c,d} and Renata Zukanovich Funchal^b

^a*Laboratoire de Physique Théorique (Bât. 210)*

Université Paris-Sud and CNRS (UMR 8627), F-91405 Orsay-Cedex, France

^b*Instituto de Física, Universidade de São Paulo, C.P. 66.318, 05315-970 São Paulo, Brazil*

^c*Dipartimento di Fisica e Astronomia ‘G. Galilei’, Università di Padova, Italy*

^d*Istituto Nazionale Fisica Nucleare, Sezione di Padova, I-35131 Padova, Italy*

ABSTRACT: We investigate the sensitivity of IceCube(-Gen2) to a scalar leptoquark scenario with couplings only to heavy quark flavors which may be connected to solving discrepancies in B -meson semileptonic decays. We take into account, for the first time, the non-negligible neutrino-gluon cross section induced by leptoquarks, and we systematically account for indirect and direct constraints which have been overlooked in previous studies. We conclude that IceCube(-Gen2) can only probe the light LQ regime, already disfavored by the combination of flavor physics constraints, electroweak precision data and the direct searches at the LHC.

KEYWORDS: *Beyond Standard Model, Leptoquarks*

Contents

1	Introduction	1
2	A Simple Leptoquark Scenario to Explain $R_{D^{(*)}}$	4
2.1	R_2 explanation of $R_{D^{(*)}}$	4
2.2	General Constraints	6
2.2.1	Constraints from Z decays	6
2.2.2	Limits from Direct Detection	8
3	High Energy Neutrino Events in IceCube	10
3.1	Calculation of the Event Rate in IceCube	12
3.2	Leptoquark Contribution to the Event Rate	13
3.3	Attenuation and Regeneration Effects	16
4	Statistical Data Analysis at IceCube, Present and Future	16
4.1	Current Data Analysis	17
4.2	Future IceCube(-Gen2) Projections	18
5	Conclusions	19
A	Leptoquark Contributions to the Neutrino-Nucleon Scattering Cross Section	22
A.1	ν_ℓ -gluon contribution	22
A.2	ν_ℓ -quark contribution	23
B	Transport Equations Including the Leptoquark Contribution	24
C	$B \rightarrow D\ell\bar{\nu}$ expressions	25

1 Introduction

It is remarkable that the two types of constituents in the flavor sector of the Standard Model (SM), quarks and leptons, although independent, share a number of common features. They come in three generations that conspire to exactly cancel the triangle anomalies of the gauge interactions, they exhibit mixing between mass and flavor eigenstates resulting in oscillations, and flavor changing neutral interactions do not occur at tree-level. These common features strongly suggest that quarks and leptons should be somehow interrelated. In fact, leptoquarks (LQs), bosons that can mediate quark-lepton transitions, appear in many extensions of the SM, in particular, in Grand Unified Theories [1, 2], and composite Higgs models [3–5].

From a phenomenological point of view, LQs are $SU(3)_c$ colored particles that can come as $SU(2)_L$ singlets, doublets or triplets [6, 7]. Their masses, strength and flavor structure of their couplings to quarks and leptons are all undetermined when the ultraviolet completion is unknown. Since LQs with masses of the order of the electroweak scale are not disallowed by any fundamental reason, it is important to look for them in all possible ways. In fact, many collider experiments have been searching for them in pair as well as in single production modes. From HERA to the LHC, experiments have been setting stringent limits on their masses and couplings, c.f. [8, 9] and references therein. These limits depend, unfortunately, unavoidably on the assumed flavor structure, some of which are difficult to explore in accelerators. Other bounds deduced from the direct searches have been discussed in Ref. [10], see also references therein.

Besides the purely theoretical reasons that compel experimentalists to look for these particles it seems there might be an experimental one too, coming from B -physics. The excellent agreement between the SM predictions and experimental data seems to be disrupted by flavor physics. Recent data from the LHC, Belle and BaBar suggest lepton flavor universality violation (LFUV) in B -meson semileptonic decays. The LHCb experiment, for instance, has reported about 2.6σ discrepancy in the ratio of the partial branching fractions of the loop induced transitions (denoted by \mathcal{B}'),

$$R_{K^{(*)}}^{\text{exp}} = \frac{\mathcal{B}'(B \rightarrow K^{(*)}\mu^+\mu^-)}{\mathcal{B}'(B \rightarrow K^{(*)}e^+e^-)}, \quad (1.1)$$

and the measured values [11, 12] appear to be smaller than predicted in the SM [13, 14]. Another intriguing indication of LFUV comes from the tree-level ratio [15]

$$R_D^{\text{exp}} = \frac{\mathcal{B}(B \rightarrow D\tau\nu)}{\mathcal{B}(B \rightarrow D\ell\nu)} = 0.41 \pm 0.05, \quad (1.2)$$

where $\ell = e, \mu$, obtained by combining Babar and Belle results [16–20] and 2.2σ above $R_D^{\text{SM}} = 0.300(8)$, the SM prediction [15, 21, 22]. This feature was confirmed with $R_{D^*}^{\text{exp}} = 0.304(15)$ [16, 17, 23], which also appears about 3σ larger than the SM prediction, $R_{D^*}^{\text{SM}} = 0.260(8)$ [24, 25]. Another confirmation of this phenomenon was reported by LHCb who measured $R_{J/\psi} = \mathcal{B}(B_c \rightarrow J/\psi\tau\nu)/\mathcal{B}(B_c \rightarrow J/\psi\mu\nu) = 0.71 \pm 0.25$ [26], also larger than the SM estimates although the SM value in this case is less reliable. Many proposed solutions to these anomalies discussed in the literature so far rely on existence of LQ states [27–54], notice that similar solutions can be implemented by considering supersymmetric models including R-Parity violating squarks [55]. The couplings of LQs to heavy quarks can be as peculiar as to make them difficult for direct observations in colliders and it is therefore useful to try and look for them in other ways.

Here we study a possibility of using the IceCube neutrino telescope in the South Pole as a complementary way to search for those states. Many authors have explored the potential of IceCube to test LQ models, in particular, after the observation of an excess of high energy starting events consistent with a flux of high-energy astrophysical neutrinos from outside our galaxy [56]. In Ref. [57] electroweak singlet LQ that couple to either

second or third generation of quarks and/or leptons were studied, emphasizing the use of the inelasticity distribution of events to improve background rejection. Refs. [58], [59] and [60] evoke LQ couplings to the first generation of quarks and leptons in order to try to accommodate IceCube high-energy neutrino data. Similarly, in [64] a supersymmetric model including R-parity violating squark resonances is considered to explain IceCube data. The limits that IceCube data can impose on a specific low-scale quark-lepton unification model with scalar LQs was studied in [61]. Scalar LQ doublets that couple the first and third family of quarks to leptons, with a flavor structure that can address the anomalies in $R_{K^{(*)}}$, pass other LHC constraints and give a sizable contribution to IceCube neutrino data were considered in [62] and by a more elaborated analysis in [63]. The LQ states in all of these works, with exception of Ref. [57], couple to the first generation of quarks. Couplings to the first generation suffer, however, from severe experimental constraints as they have to comply with limits from direct searches at colliders, atomic parity violation experiments and flavor physics observables in the kaon/pion sectors. Moreover, all previous studies of the neutrino-nucleon cross-section at IceCube only consider the resonant s - and t -channel interactions of high energy neutrinos with quarks (valence and/or sea) via a LQ exchange. Nonetheless, we should not forget that in order to compute neutrino-nucleon cross sections we must also include the neutrino interaction with gluons mediated by a LQ, particularly important in accessing LQs that only couple to heavy quarks. Those are, in fact, the kinds of LQs that can take part in solving the discrepancies between data and heavy meson semileptonic decays. In this paper, we include for the first time the neutrino-gluon cross-section in order to consistently study the sensitivity of IceCube to LQ scenarios. Furthermore, we systematically compare the future IceCube future sensitivity with the indirect constraints coming from flavor physics and Z -pole observables, as well as the direct limits from the LHC, which are very efficient in constraining the LQ couplings.

Our paper is organized as follows. In Sec. 2 we describe a LQ model with a particular simple flavor structure that can solve $R_{D^{(*)}}$ and give rise to new neutrino-nucleon interactions which can be probed by IceCube. Furthermore, we perform a complete study of the indirect bounds on LQ couplings stemming from flavor physics and Z -pole observables. In Sec. 3 we review the High Energy Starting Events sample collected by IceCube after six years and we discuss the current status of the SM fit. We explain the procedure to simulate both the SM and LQ events at IceCube in order to compare with experimental data. In Sec. 4 we present results of our analysis and discuss what we can learn about our model from six years of IceCube data as well as the prospects for what can be expected in the future. We finally conclude in Sec. 5. All LQ contributions to the neutrino-nucleon scattering cross section, including the new ones, are collected in Appendix A, while in Appendix B we describe the transport equation for Earth's attenuation. The decay rate expressions for $B \rightarrow D\ell\bar{\nu}$ are provided in Appendix C.

2 A Simple Leptoquark Scenario to Explain $R_{D^{(*)}}$

In this paper we focus on the so called R_2 -model which involves an electroweak doublet of scalar LQs with hypercharge $Y = 7/6$, described by the Yukawa Lagrangian,

$$\begin{aligned}\mathcal{L}_{\Delta^{(7/6)}} &= (g_R)_{ij} \bar{Q}_i \Delta^{(7/6)} \ell_{Rj} + (g_L)_{ij} \bar{u}_{Ri} \tilde{\Delta}^{(7/6)\dagger} L_j + \text{h.c.} \\ &= (V g_R)_{ij} \bar{u}_i P_R \ell_j \Delta^{(5/3)} + (g_R)_{ij} \bar{d}_i P_R \ell_j \Delta^{(2/3)} \\ &\quad + (g_L U)_{ij} \bar{u}_i P_L \nu_j \Delta^{(2/3)} - (g_L)_{ij} \bar{u}_i P_L \ell_j \Delta^{(5/3)} + \text{h.c.},\end{aligned}\tag{2.1}$$

where in the first line the Lagrangian is given in the flavor basis and the superscripts in the LQ fields refer to the hypercharge (Y), while in the other two lines the Lagrangian is given in the mass eigenstate basis in which the superscripts of LQs refer to the electric charge $Q = Y + T_3$, where Y is the hypercharge and T_3 the third component of weak isospin. Note that $\tilde{\Delta} = i\tau_2 \Delta^*$ is the conjugate of the doublet of mass degenerate LQs, while V and U stand for the Cabibbo-Kobayashi-Maskawa (CKM) and the Pontecorvo-Maki-Nakagawa-Sakata (PMNS) matrices, respectively. Furthermore, $P_{L,R} = (1 \mp \gamma_5)/2$ are the chiral projectors, $Q_i = [(V^\dagger u_L)_i \ d_{Li}]^T$ and $L_i = [(U \nu_L)_i \ \ell_{Li}]^T$ denote quark and lepton $SU(2)_L$ doublets, whereas u_L , d_L , ℓ_L and ν_L are the fermion mass eigenstates.

We opt for the minimalistic structure of the Yukawa coupling matrices $g_{L,R}$ and assume

$$g_L = \begin{pmatrix} 0 & 0 & 0 \\ 0 & 0 & g_L^{c\tau} \\ 0 & 0 & 0 \end{pmatrix}, \quad g_R = \begin{pmatrix} 0 & 0 & 0 \\ 0 & 0 & 0 \\ 0 & 0 & g_R^{b\tau} \end{pmatrix}, \quad V g_R = \begin{pmatrix} 0 & 0 & V_{ub} g_R^{b\tau} \\ 0 & 0 & V_{cb} g_R^{b\tau} \\ 0 & 0 & V_{tb} g_R^{b\tau} \end{pmatrix},\tag{2.2}$$

that allows $\Delta^{(2/3)}$ to mediate a tree-level contribution to $R_{D^{(*)}}$ and generates a contribution to the neutrino-nucleon scattering in IceCube.

2.1 R_2 explanation of $R_{D^{(*)}}$

In order to confront the LQ contributions with the experimental data involving the $B \rightarrow D\tau\nu$ decay we consider the effective Hamiltonian

$$\begin{aligned}\mathcal{H}_{\text{eff}} &= \frac{4G_F}{\sqrt{2}} V_{cb} \left[(\bar{\tau}_L \gamma^\mu \nu_L) (\bar{c}_L \gamma_\mu b_L) + g_S(\mu) (\bar{\tau}_R \nu_L) (\bar{c}_R b_L) \right. \\ &\quad \left. + g_T(\mu) (\bar{\tau}_R \sigma^{\mu\nu} \nu_L) (\bar{c}_R \sigma_{\mu\nu} b_L) \right] + \text{h.c.},\end{aligned}\tag{2.3}$$

where $g_{S,T}$ are the Wilson coefficients induced by the LQ state mediating the semileptonic decay via a tree-level contribution shown in Fig. 1. After integrating out $\Delta^{(2/3)}$, the expression for $g_{S,T}$, at the matching scale $\mu = m_\Delta$, reads:

$$g_S(\mu = m_\Delta) = 4g_T(\mu = m_\Delta) = \frac{g_L^{c\tau} (g_R^{b\tau})^*}{4\sqrt{2} m_\Delta^2 G_F V_{cb}},\tag{2.4}$$

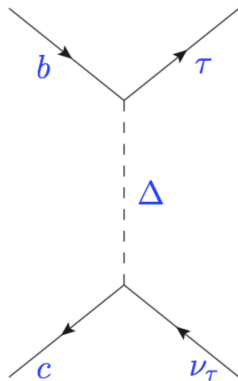


Figure 1. Contribution to $b \rightarrow c\tau\bar{\nu}_\tau$ arising from the LQ model discussed in this paper. $\Delta \equiv \Delta^{(2/3)}$ stands for the LQ.

clearly enhanced by V_{cb}^{-1} . By virtue of the leading order QCD running from $\mu = m_\Delta \approx 1$ TeV down to $\mu = m_b$, the above relation between g_S and g_T becomes

$$g_S(\mu = m_b) \approx 7.2 \times g_T(\mu = m_b). \quad (2.5)$$

Furthermore, we included the small electroweak corrections discussed in Ref. [65] which can induce mixing between the scalar and tensor contributions.

We focus on $B \rightarrow D$ semileptonic decays for which the hadronic form factors have been computed by means of numerical simulations of QCD on the lattice in Refs. [21, 22].¹ To fill the discrepancy between R_D^{SM} and R_D^{exp} one then allows for $g_S \neq 0$. In this way we find the region of allowed values of $\text{Re}[g_S(m_b)]$ and $\text{Im}[g_S(m_b)]$ which is depicted by the blue regions in Fig. 2 to 1, 2 and 3σ accuracy. We decided not to include R_{D^*} in the same fit because the lattice QCD determination of the form factors at non-zero recoil has not been made, in addition to the fact that the relevant pseudoscalar form factor has never been computed on the lattice. To verify that our solution to R_D also gives an improvement of R_{D^*} , despite the uncertainties mentioned above which need to be clarified by lattice simulations, we show in the same plot the 2σ region consistent with $R_{D^*}^{\text{exp}}$. The latter region was obtained by using the $B \rightarrow D^*\ell\nu_\ell$ form factors extracted from experimental results [15], combined with the ratio $A_0(q^2)/A_1(q^2)$ and $T_{1-3}(q^2)/A_1(q^2)$ computed in Ref. [66]. By using this approach, we conclude that, in the R_2 -model, only the complex g_S solutions to R_D can provide a reasonable agreement with $R_{D^*}^{\text{exp}}$, a fact that agrees with findings of Ref. [67]. Therefore, we will focus our analysis on the solutions to R_D with complex Wilson coefficients

$$|g_S(\mu = m_b)| \in (0.56, 0.74), \quad (2.6)$$

obtained to 1σ accuracy. This relation implies that the magnitude of LQ couplings should be such that

$$\frac{|g_L^{c\tau}||g_R^{b\tau}|}{m_\Delta^2} \in (0.80, 1.32) \times (1 \text{ TeV})^{-2}, \quad (2.7)$$

¹For the reader's convenience we provide in Appendix C the expression for the $B \rightarrow D\ell\bar{\nu}$ decay rate.

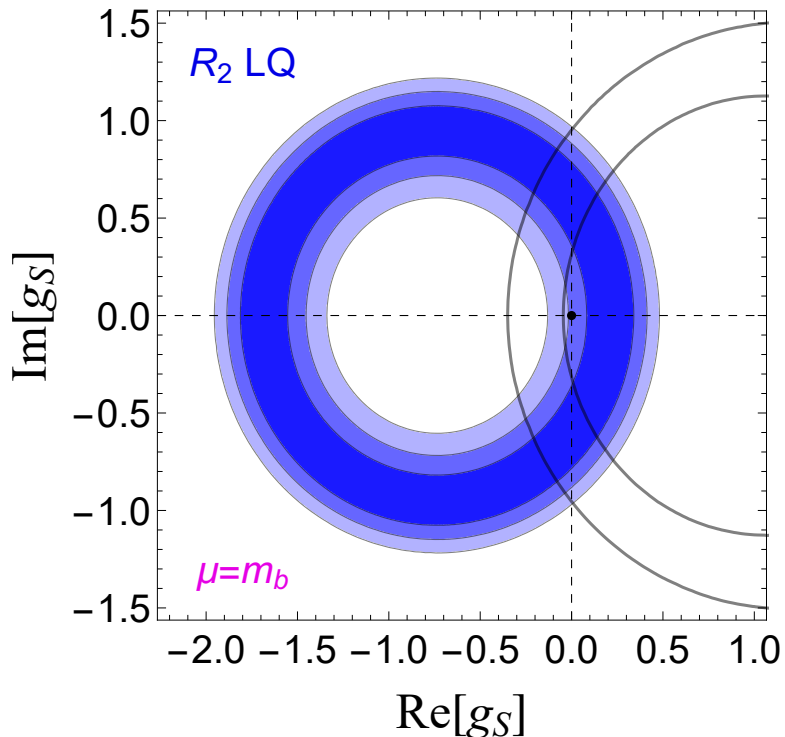


Figure 2. Regions of allowed values for $g_S(\mu = m_b)$ on the complex plane, compatible with experimentally measured R_D to 1-, 2- and 3 σ (from darker to lighter blue). We assumed $g_S(\mu = m_\Delta) = 4 \times g_T(\mu = m_\Delta)$, as predicted by the R_2 LQ scenario, and considered the QCD running from $\mu \approx 1$ TeV to m_b , cf. Eq. (2.5). We also show in black the region compatible to 2 σ accuracy with $R_{D^{(*)}}^{\text{exp}}$, which indicates that the effective couplings must be complex in this scenario. See discussion in the text.

where we used $|V_{cb}| = 0.0417(20)$ [68]. We see that the couplings needed to explain R_D for $m_\Delta \lesssim 1$ TeV should not be too large, mostly due to the CKM enhancement in Eq. (2.4).

In the following we show that the explanation of $R_{D^{(*)}}^{\text{exp}} > R_{D^{(*)}}^{\text{SM}}$ described above is consistent with other limits from flavor physics and the direct searches for pair-produced LQs at the LHC. To that purpose, we will assume that the coupling $g_R^{b\tau}$ is purely imaginary.

2.2 General Constraints

The choice of $g_L^{c\tau} \neq 0$ and $g_R^{b\tau} \neq 0$ in Eq. (2.2) allows us to avoid many flavor physics constraints, making this explanation of $R_{D^{(*)}}^{\text{exp}} > R_{D^{(*)}}^{\text{SM}}$ particularly simple. Processes mediated by the flavor-changing neutral $\Delta F = 1$ and $\Delta F = 2$ currents are not altered in this scenario. Only the charged-current transitions $b \rightarrow c\tau\bar{\nu}$ are modified, as desired. The most significant constraints to this scenario actually come from the Z boson decay widths.

2.2.1 Constraints from Z decays

Our LQ model induces modifications to Z -boson decays through loop contributions, as depicted in Fig. 3. Those effects have to be consistent with the LEP measurements of

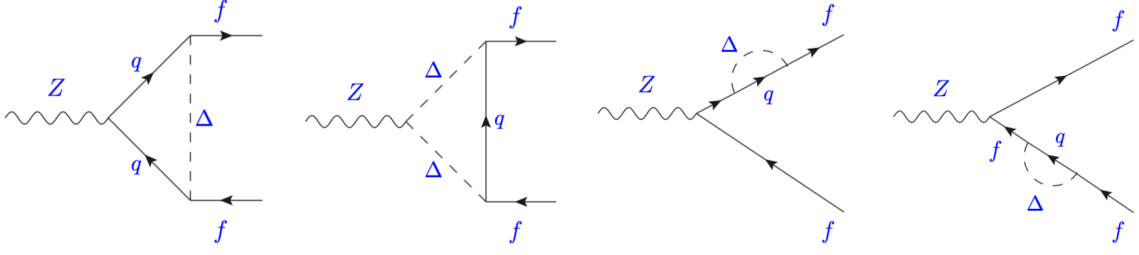


Figure 3. Contributions to the $Z \rightarrow f\bar{f}$ decay amplitude generated in our R_2 model, where the LQ Δ is either $\Delta^{(2/3)}$ or $\Delta^{(5/3)}$, $q \in \{u, c, b, t\}$ depending on the LQ state running in the loop, while f is either ℓ or ν . Similar diagrams can be drawn for $Z \rightarrow b\bar{b}$.

$\mathcal{B}(Z \rightarrow \ell^+\ell^-)$ [69]. The Lagrangian describing the $Zf\bar{f}$ coupling can be written as

$$\mathcal{L}_{Zf\bar{f}} = \frac{g}{\cos\theta_W} Z^\mu \bar{f} \gamma_\mu \left(g_L^f P_L + g_R^f P_R \right) f, \quad (2.8)$$

where g is the $SU(2)_L$ gauge coupling, and

$$\begin{aligned} g_L^f &= g_L^{f,\text{SM}} + \delta g_L^f, \\ g_R^f &= g_R^{f,\text{SM}} + \delta g_R^f, \end{aligned} \quad (2.9)$$

where $g_L^{f,\text{SM}} = T_3 - Q \sin^2\theta_W$ and $g_R^{f,\text{SM}} = -Q \sin^2\theta_W$ are the SM contributions, while $\delta g_{L,R}^f$ parametrize LQ loop contributions. The corresponding branching ratio is then given by

$$\mathcal{B}(Z \rightarrow f\bar{f}) = \frac{m_Z^3}{6\pi v^2 \Gamma_Z} \beta_f \left[\left[|g_L^f|^2 + |g_R^f|^2 \right] \left(1 - \frac{m_f^2}{m_Z^2} \right) + \frac{6m_f^2}{m_Z^2} \text{Re} \left(g_L^f g_R^{f*} \right) \right], \quad (2.10)$$

where m_f is the fermion mass and $\beta_f = \sqrt{1 - 4m_f^2/m_Z^2}$.

The LQ couplings lead to up- and down-type quark loop contributions to $\delta g_{L(R)}^\tau$, which are given by

$$\begin{aligned} \delta g_R^\tau &= N_c |g_R^{b\tau}|^2 \left\{ |V_{tb}|^2 \frac{x_t}{32\pi^2} (1 + \log x_t) \right. \\ &+ \frac{x_z}{144\pi^2} \left[- \left(\sin^2\theta_W - \frac{3}{2} \right) (\log x_z + i\pi) + \left(-\frac{1}{4} + \frac{2}{3} \sin^2\theta_W \right) \right] \\ &\left. + (1 - |V_{tb}|^2) \frac{x_z}{72\pi^2} \left[\left(\sin^2\theta_W - \frac{3}{4} \right) \left(\log x_z + i\pi + \frac{1}{12} \right) + \frac{3}{16} \right] \right\}, \end{aligned} \quad (2.11)$$

and

$$\delta g_L^\tau = N_c |g_L^{c\tau}|^2 \frac{x_z}{72\pi^2} \left[\sin^2\theta_W \left(\log x_z + i\pi + \frac{1}{12} \right) - \frac{1}{8} \right], \quad (2.12)$$

where $x_t = m_t^2/m_\Delta^2$ and $x_z = m_Z^2/m_\Delta^2$, and $N_c = 3$ is the number of colors.² The dominant term in δg_R^τ comes from the top quark since it enhances the loop function. The effective coupling δg_L^τ does not exhibit a similar mass enhancement, and it is for this reason less relevant for phenomenology. Similarly, the LQ interaction with the charm quarks also induces an effective coupling to τ neutrinos, which reads

$$\delta g_L^{\nu\tau} = N_c |g_L^{c\tau}|^2 \frac{x_z}{72\pi^2} \left[\sin^2 \theta_W \left(\log x_z + i\pi - \frac{1}{6} \right) + \frac{1}{8} \right]. \quad (2.13)$$

The effective couplings given above are constrained by the LEP measurements of the Z decay widths and other electroweak observables [69]. The measurements of the effective Z couplings give [70],

$$\frac{g_V^\tau}{g_V^e} = 0.959(29), \quad \frac{g_A^\tau}{g_A^e} = 1.0019(15), \quad (2.14)$$

where $g_{V(A)}^f = g_L^f \pm g_R^f$. These results translate into useful bounds on the LQ contributions to $\delta g_{L,R}^\tau$. Furthermore, the LEP bound on the effective number of neutrinos [70]

$$N_\nu = 2.9840(82), \quad (2.15)$$

will constrain the LQ couplings via the expression,

$$N_\nu = 2 + \left| 1 + \frac{\delta g_L^{\nu\tau}}{g_L^{\nu\tau, \text{SM}}} \right|^2. \quad (2.16)$$

As we shall see below, the coupling $g_R^{b\tau}$ is tightly limited by $\mathcal{B}(Z \rightarrow \tau\tau)$ due to the enhancement of the loop function by the top quark mass. On the other hand, the constraints on $g_L^{c\tau}$ derived from N_ν would be relevant only for very light LQ states, already excluded by the constraints stemming from $g_{V,A}^\tau$. Finally, we have also checked that the bound on the LQ couplings arising from $\mathcal{B}(Z \rightarrow b\bar{b})$ is not significant with current experimental precision.

2.2.2 Limits from Direct Detection

Direct searches at the LHC for pair-produced LQs provide useful limits on the couplings $g_L^{c\tau}$ and $g_R^{b\tau}$ as a function of the LQ mass m_Δ . For the flavor ansatz given in Eq. (2.2) the allowed LQ decay modes are

$$\begin{aligned} \Delta^{(2/3)} &\rightarrow c\nu, \quad b\tau, \\ \Delta^{(5/3)} &\rightarrow u\tau, \quad c\tau, \quad t\tau. \end{aligned} \quad (2.17)$$

The CMS collaboration recently improved bounds of LQs decaying to $b\tau$, obtaining a lower bound on m_Δ of 900 GeV, with the assumption $\mathcal{B}(\Delta^{(2/3)} \rightarrow b\tau) = 1$ [71, 72]. Similarly, CMS

²One can easily identify the top and bottom quark contributions in the first two lines of Eq. (2.11), while the ones coming from the up and charm quarks have been recast in the same equation by using the unitarity of V_{CKM} , i.e. $|V_{ub} g_R^{b\tau}|^2 + |V_{cb} g_R^{b\tau}|^2 = |g_R^{b\tau}|^2 (1 - |V_{tb}|^2)$.

excludes LQs decaying into $t\tau$ with masses $m_\Delta \gtrsim 850$ GeV if $\mathcal{B}(\Delta^{(5/3)} \rightarrow t\tau) = 1$ [73, 74]. Furthermore, a search for pair-produced LQs decaying into a light quark ($q = u, d, s, c$) and a neutrino has been reported by CMS, allowing us to set the limit $m_\Delta \gtrsim 980$ GeV if $\mathcal{B}(\Delta^{(2/3)} \rightarrow c\nu) = 1$ [75].

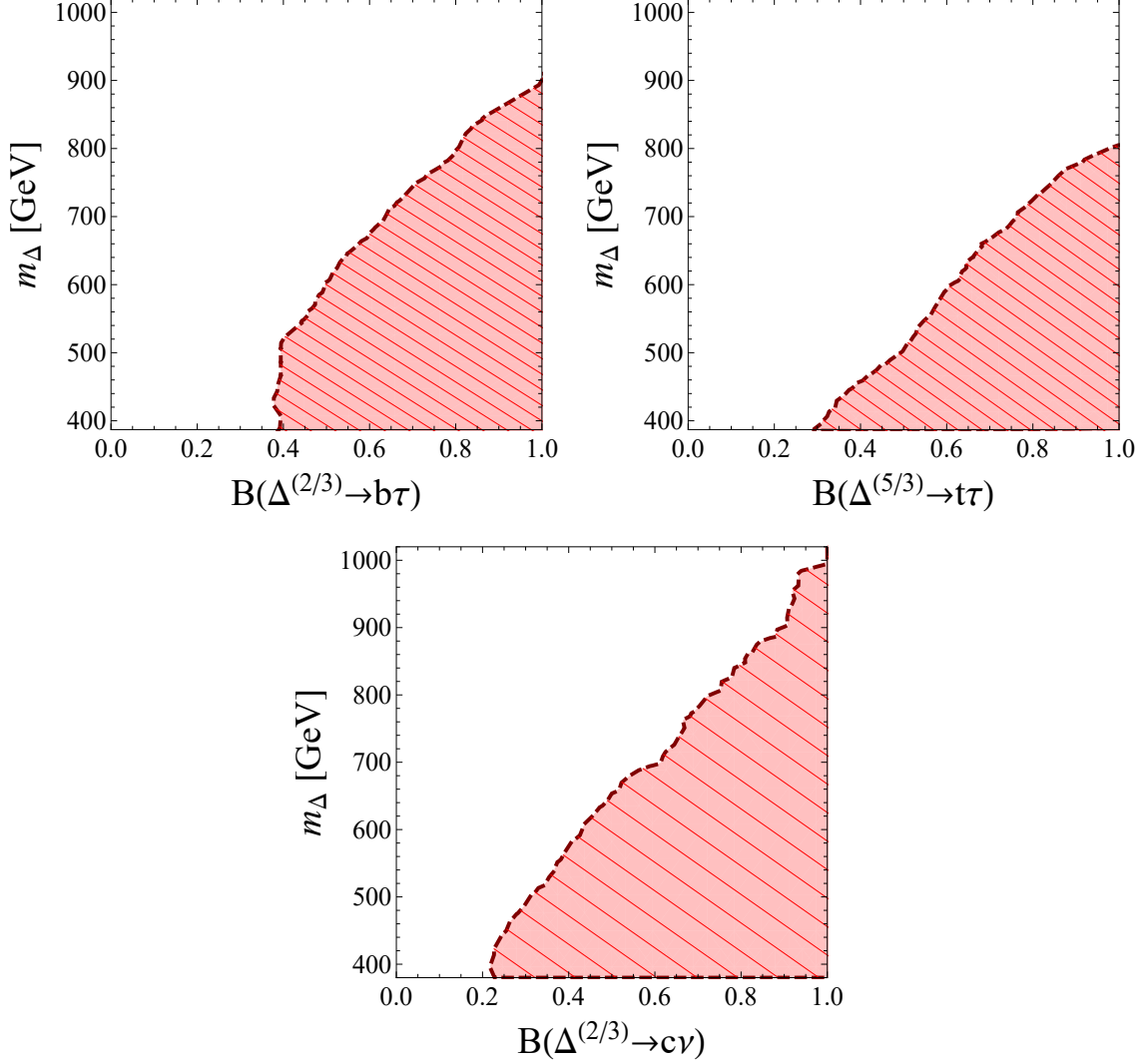


Figure 4. Exclusion regions of m_Δ as a function of $\mathcal{B}(\Delta^{(2/3)} \rightarrow b\tau)$ [71, 72], $\mathcal{B}(\Delta^{(5/3)} \rightarrow t\tau)$ [73, 74] and $\mathcal{B}(\Delta^{(2/3)} \rightarrow c\nu)$ [75] at 95% CL. See text for details.

In any realistic scenario, the limits mentioned above have to be reinterpreted to account for values of the branching ratios smaller than one. The reinterpretation of these exclusion limits on m_Δ are shown in Fig. 4 as a function of $\mathcal{B}(\Delta^{(2/3)} \rightarrow b\tau)$ (upper left panel), $\mathcal{B}(\Delta^{(5/3)} \rightarrow t\tau)$ (upper right panel) and $\mathcal{B}(\Delta^{(2/3)} \rightarrow c\nu)$ (lower panel). In the scenario we are considering, cf. Eq. (2.2), the branching ratios read

$$\mathcal{B}(\Delta^{(2/3)} \rightarrow c\nu) = \frac{|g_L^{c\tau}|^2}{|g_R^{b\tau}|^2 + |g_L^{c\tau}|^2}, \quad \mathcal{B}(\Delta^{(2/3)} \rightarrow b\tau) = \frac{|g_R^{b\tau}|^2}{|g_R^{b\tau}|^2 + |g_L^{c\tau}|^2}, \quad (2.18)$$

and

$$\mathcal{B}(\Delta^{(5/3)} \rightarrow t\tau) = \frac{|g_R^{b\tau}|^2 \left(1 - \frac{m_t^2}{m_\Delta^2}\right)^2}{|g_R^{b\tau}|^2 \left(1 - \frac{m_t^2}{m_\Delta^2}\right)^2 + |g_L^{c\tau}|^2}, \quad (2.19)$$

where, for simplicity, we assumed $|V_{tb}| \approx 1$ and neglected the light fermion masses (m_c , m_b and m_τ). From the above formulas we conclude that scenarios with $m_\Delta \lesssim 1$ TeV can comply with the limits of Fig. 4 if the branching ratios are diluted by a large coupling to the charm quark. In other words, the ratio $|g_R^{b\tau}|/|g_L^{c\tau}|$ should be of $\mathcal{O}(1)$, which also agrees with the constraints on $g_R^{b\tau}$ derived from $Z \rightarrow \tau^+\tau^-$, cf. Eq. (2.11). We checked that m_Δ can be as low as ≈ 650 GeV for some combinations of Yukawa couplings.

In Fig. 5, we confront the allowed region by R_D with the indirect and direct constraints discussed above by assuming $g_R^{b\tau}$ to be purely imaginary, as discussed in Sec. 2.1. For instance, we see in these plots that both $|g_R^{b\tau}|$ and $g_L^{c\tau}$ are bounded from above by the Z -pole observables. Furthermore, the couplings needed to explain R_D for $m_\Delta \lesssim 1$ TeV are not very large, mostly due to the CKM enhancement in Eq. (2.4), and they can therefore be perfectly consistent with phenomenological constraints discussed in this Section.

In what follows, we will discuss the IceCube phenomenology of the LQ scenario considered in this paper. In practice, we will focus on the analysis of the parameter space defined by m_Δ and $g_L^{c\tau}$ since they are the relevant parameters to determine IceCube signals. In this plane the region allowed by the Z -pole observables is approximately limited by a straight line, such that the allowed values are $g_L^{c\tau} \lesssim 1.6 + 1.3(m_\Delta/300 \text{ GeV} - 1)$, which is also illustrated in this paper in Figs. 12 and 14.

3 High Energy Neutrino Events in IceCube

The cubic kilometer IceCube Neutrino Observatory in the South Pole observed between 2010 and 2012 the first evidence of a diffuse flux of astrophysical neutrinos above 100 TeV [56], which was further confirmed in the updated analyses [76–78]. In this paper we consider the 6-year sample [78] which contains 80 High Energy Starting Events (HESE). In particular, we focus on the 28 events with deposited energies above 100 TeV, which are divided in 23 showers and 5 tracks. This flux, of yet unknown astrophysical origin, seems to be isotropic and consistent with a single power law behavior followed by neutrinos and antineutrinos of all flavors [79]. In other words, the neutrino energy spectrum can be parameterized by a spectral index, γ , and a normalization constant C_0 as

$$\frac{d\Phi_\nu}{dE_\nu} = \frac{C_0}{10^8} \left(\frac{E_\nu}{100 \text{ TeV}}\right)^{2-\gamma} \frac{1}{E_\nu^2} [\text{GeV}^{-1} \text{ cm}^{-2} \text{ str}^{-1} \text{ s}^{-1}], \quad (3.1)$$

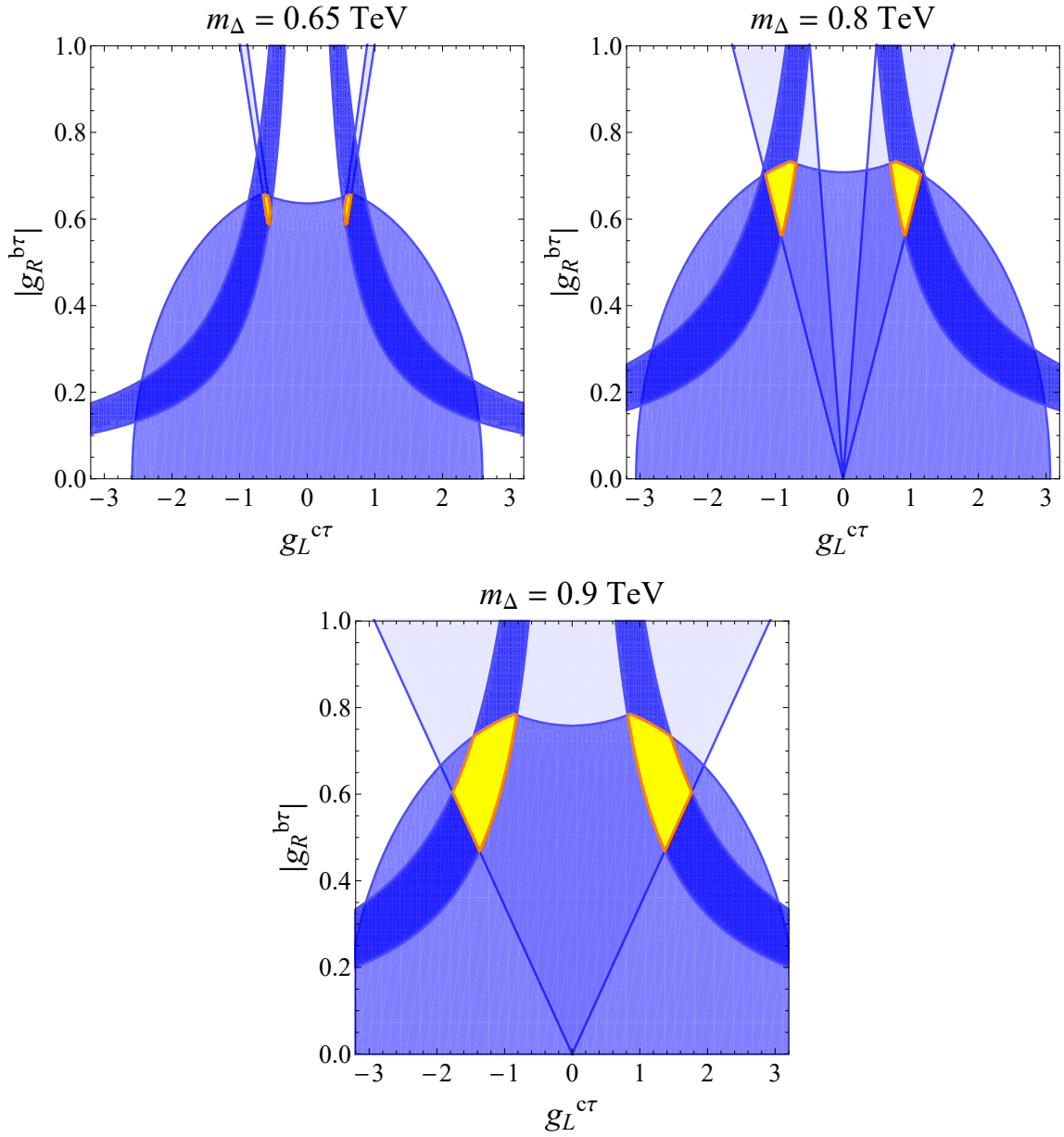


Figure 5. The allowed region on the plane $g_L^{c\tau} \times |g_R^{b\tau}|$ by current experimental constraints is shown in yellow for $m_\Delta \in \{0.65, 0.8, 0.9\}$ TeV. We assume $g_R^{b\tau}$ to be a purely imaginary coupling, as described in the text. The separate allowed regions both from the direct searches at the LHC, the Z -pole observables and R_D are shown from lighter to darker blue, respectively. Thus, the yellow region is given by their intersection. See text for details.

so that at the Earth the flavor fluxes are given by

$$\frac{d\Phi_\alpha}{dE_\nu} = f_\alpha^\oplus \frac{d\Phi_\nu}{dE_\nu}, \quad (3.2)$$

where f_{α}^{\oplus} , $\alpha = \{\nu_e, \nu_{\mu}, \nu_{\tau}, \bar{\nu}_e, \bar{\nu}_{\mu}, \bar{\nu}_{\tau}\}$, are the normalized neutrino and antineutrino flavor fractions at the Earth.

Assuming the flavor composition to be the standard one expected from neutrino oscillations, *i.e.*, $(f_{\nu_e}^{\oplus} : f_{\nu_{\mu}}^{\oplus} : f_{\nu_{\tau}}^{\oplus}) = (f_{\bar{\nu}_e}^{\oplus} : f_{\bar{\nu}_{\mu}}^{\oplus} : f_{\bar{\nu}_{\tau}}^{\oplus}) = (1 : 1 : 1)$, IceCube best fit of 6-year sample yields $\gamma = 2.92_{-0.29}^{+0.33}$ and $C_0 = 2.46 \pm 0.8 \text{ GeV cm}^{-2} \text{ str}^{-1} \text{ s}^{-1}$ [78]. To test our fitting procedure we used the publicly available IceCube data, fit them to the SM and obtained ³

$$\gamma = 2.98_{-0.38}^{+0.42}, \quad C_0 = 2.63_{-1.23}^{+1.87} \text{ GeV cm}^{-2} \text{ str}^{-1} \text{ s}^{-1} \quad (3.3)$$

with a p-value of 0.25, in full agreement with the above-mentioned IceCube results [78]. The best fit curves for shower and track spectra are shown in Fig. 6. ⁴ For simplicity, in the fit we have used a fixed atmospheric background spectrum which is derived from the central values for the total amount of atmospheric neutrinos estimated in [78], which are $N_{\mu} = 25.2 \pm 7.3$ and $N_{\text{atm}} = 15.6_{-0.3.9}^{+11.4}$. To reduce the effects of uncertainties we focus on the energy range [100 TeV, 10 PeV], in which the background contribution is sub-leading. Indeed, the computation of the best fit considering the minimum (maximum) expectations for the atmospheric background yields $\gamma = 3.0(2.9)$ and $C_0 = 2.7(2.4)$ with a p-value of 0.24 (0.23), which lies perfectly inside the allowed 1σ region. We will apply the same strategy to analyze LQ scenarios. Before passing onto that discussion we examine some aspects of the simulation of IceCube events, with special attention to the new contributions introduced by LQ interactions.

3.1 Calculation of the Event Rate in IceCube

Icecube detects individual neutrino events through the Cherenkov radiation emitted by charged secondary particles produced in the neutrino interaction with the Antarctic ice. These events are characterized by the electromagnetic (EM) equivalent of the total deposited energy in the detector (E_{dep}) and their topology (track or shower). Within the SM, track events can only arise when ν_{μ} or $\bar{\nu}_{\mu}$ interact with nucleons via charged current (CC) interactions, producing a energetic muon or antimuon. On the other hand, shower events can be induced by CC interactions of $\bar{\nu}_e$ and $\bar{\nu}_{\tau}$ or by neutral current (NC) interactions of all (anti-)neutrino flavors with nucleons.

To calculate the number of shower (sh) or track (tr) events produced by SM interactions in an interval of reconstructed energy $[E_{\text{dep}}, E_{\text{dep}} + dE_{\text{dep}}]$, we first calculate the individual

³The details about our statistical analysis considering the SM and several LQ scenarios are explained in Section 4. We advance the results from the best fit of the SM in this section both to visualize graphically the IceCube 6-year dataset, Fig. 6, and also to establish some general but important remarks about the analysis.

⁴Notice that the contribution of the atmospheric background to the neutrino spectrum, which we obtain by using the modelling of Ref. [81], is consistent with the results shown in Ref. [78] concerning absolute numbers and spectrum shape. However, the validity of the model is challenged at low energies, for instance by the discrepancy in the number of tracks around 30 TeV, which can be treated in a way discussed in Refs. [63, 91]. Note that in this work we focus on the events above 100 TeV and rely on the validity of the atmospheric background model at high energies.

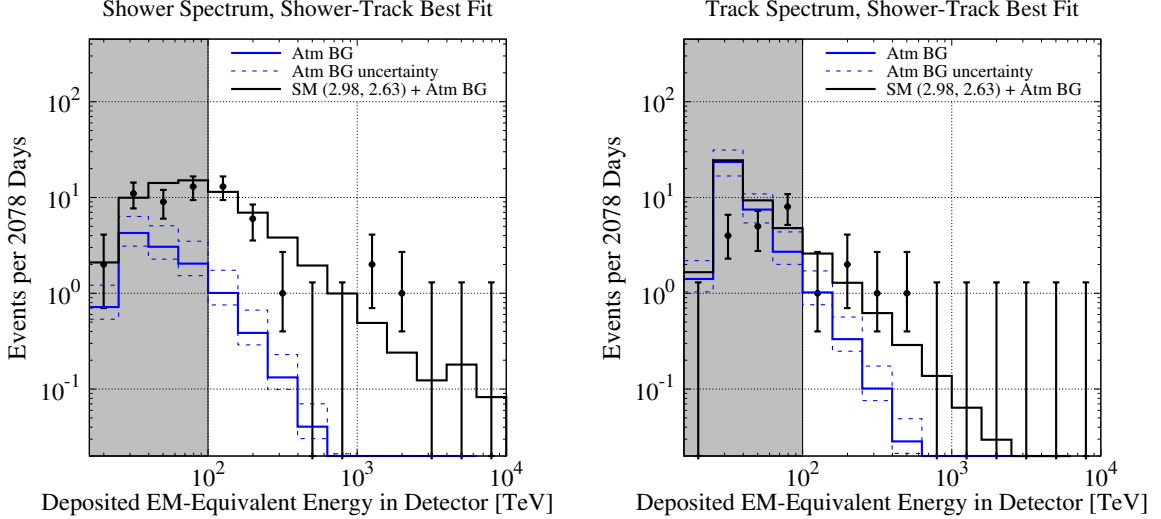


Figure 6. Standard Model best fit of the IceCube 6-year dataset in the energy range [100 TeV, 10 PeV], which gives the values $\gamma = 2.98$ and $C_0 = 2.63 \text{ GeV cm}^{-2} \text{ str}^{-1} \text{ s}^{-1}$ for the neutrino flux parameters. The atmospheric background is computed from the estimated central values given in Ref. [78], from which we obtained $N_\mu = 25.2$ and $N_{\text{atm}} = 15.6$. The points in the grey region are not included in the fit, as discussed in the text.

contributions to the event rate via the expression,

$$\frac{dN_\alpha^{\text{c,h,X}}}{dE_{\text{dep}}} = TN_A \int_0^\infty dE_\nu \mathcal{A}_\alpha^{\text{h}}(E_\nu) \frac{d\Phi_\alpha}{dE_\nu} \int_0^1 dy \mathcal{M}_{\text{eff}}(E_t) R(E_t, E_{\text{dep}}, \sigma_{E_t}) \frac{d\sigma_\alpha^{\text{X}}}{dy}, \quad (3.4)$$

where $c = \text{sh, tr}$ indicates the type of topology, $h = \text{S, N}$ the events entering the detector from the south (S) or north (N) hemisphere, and $X = \text{NC, CC, e-scattering}$ stands for the different type of processes we consider. Here, T is the exposure time in seconds, $N_A = 6.022 \times 10^{23} \text{ g}^{-1}$ is the Avogadro's number times the number of moles per each gram of protons/neutrons, and $\mathcal{A}_\alpha^{\text{h}}$ accounts for the effect of Earth's attenuation, c.f. Eq.(3.3). The effective mass of the detector in grams is denoted by $\mathcal{M}_{\text{eff}}(E_t)$, which corresponds to the mass of the target material convoluted with the efficiency of converting an event with true deposited energy E_t into the observed signal. The resolution function, $R(E_t, E_{\text{dep}}, \sigma_{E_t})$, is taken to be a Gaussian distribution with mean equal to the true deposited energy E_t and standard deviation σ_{E_t} , both clearly dependent on the particular process taking place. Finally, $d\sigma_\alpha^{\text{X}}/dy$ is the differential cross section for process X in the inelasticity interval $[y, y + dy]$. Our calculations were performed in the same way as described in Refs. [80] and [81], and we refer to these papers for further details.

3.2 Leptoquark Contribution to the Event Rate

In our model, only the coupling $g_L^{c\tau}$ affects the neutrino-nucleon production cross section at IceCube, c.f. Eq. (2.1). The other coupling, $g_R^{b\tau}$, only contributes to the total decay width of the LQ bosons. In this case, since the new interactions only involves quarks, neutrinos

and τ -leptons, this scenario will only produce nonstandard shower-like events in IceCube. The event rate with ν_τ in Eq. (3.4) will then receive the New Physics contribution

$$\frac{dN_{\nu_\tau}^{\text{sh,h},\Delta}}{dE_{\text{dep}}} = TN_A \int_0^\infty dE_\nu \mathcal{A}_{\nu_\tau}^{\text{h}}(E_\nu) \frac{d\Phi_{\nu_\tau}}{dE_\nu} \int_{y_{\text{min}}}^{y_{\text{max}}} dy \mathcal{M}_{\text{eff}}(E_t) R(E_t, E_{\text{dep}}, \sigma_{E_t}) \frac{d\sigma_{\nu_\tau}^\Delta}{dy}, \quad (3.5)$$

where the differential cross-section expressions $d\sigma_{\nu_\tau}^\Delta/dy$ can be found in Appendix A, with y being the inelasticity variable. The same expression applies *mutatis mutandis* to the $\bar{\nu}_\tau$ event rate.

In previous LQ studies [57–63], only the parton level processes $\nu_\ell + \bar{q} \rightarrow \nu_\ell + \bar{q}$ were considered in the cross-section, c.f. Fig. 7. In addition to the interaction with quarks, high-energy neutrinos can also interact with gluons via the transition $\nu_\ell + g \rightarrow q_u + \Delta$, with the LQ decaying inside the detector, as shown in Fig. 8. This contribution to the cross-section can be of the same order of the $\nu_\ell + q$ contribution when dealing with heavy quarks, $q \in \{c, b\}$, and thus cannot be neglected, as we illustrate in Fig. 9. This can be understood from the suppression of the s - and t -channel interactions with heavy quarks by the small values of the parton distribution functions (PDFs). Furthermore, the gluon PDF shows a fast growth when the Bjorken scale variable x approaches zero, giving a non-negligible contribution to heavy quark cross-sections.

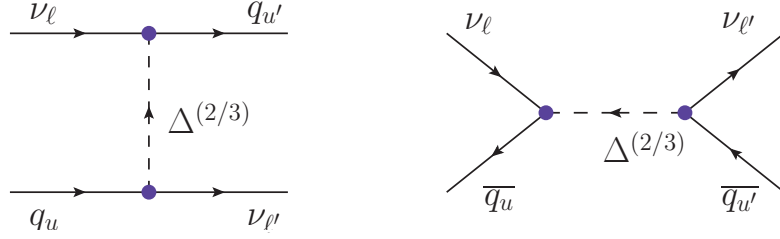


Figure 7. Feynman diagrams contributing to $\nu_\ell + q_u \rightarrow \nu_{\ell'} + q_{u'}$ and $\nu_\ell + \bar{q}_u \rightarrow \nu_{\ell'} + \bar{q}_{u'}$ via a LQ exchange. Here $\nu_\ell, \nu_{\ell'}$ are generic neutrino flavors and $q_u, q_{u'}$ are generic up-type quarks.

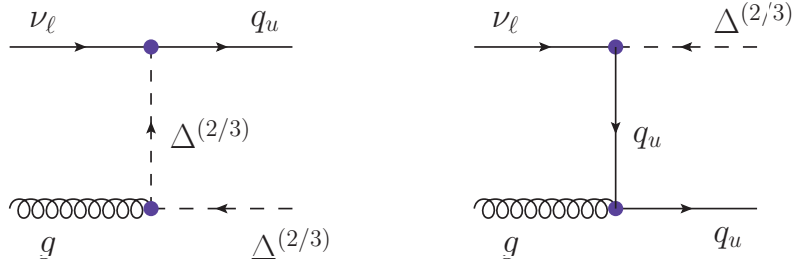


Figure 8. Feynman diagrams contributing to the process $g + \nu_\ell \rightarrow q_u + \Delta$, where the LQ particle decays into $\bar{q}_u + \nu_{\ell'}$.

To estimate the impact of LQ interactions to the IceCube data we compare in Fig. 10 the distribution of shower and track events generated by the SM and two representative LQ scenarios. These results were obtained under the restriction of a fixed total number

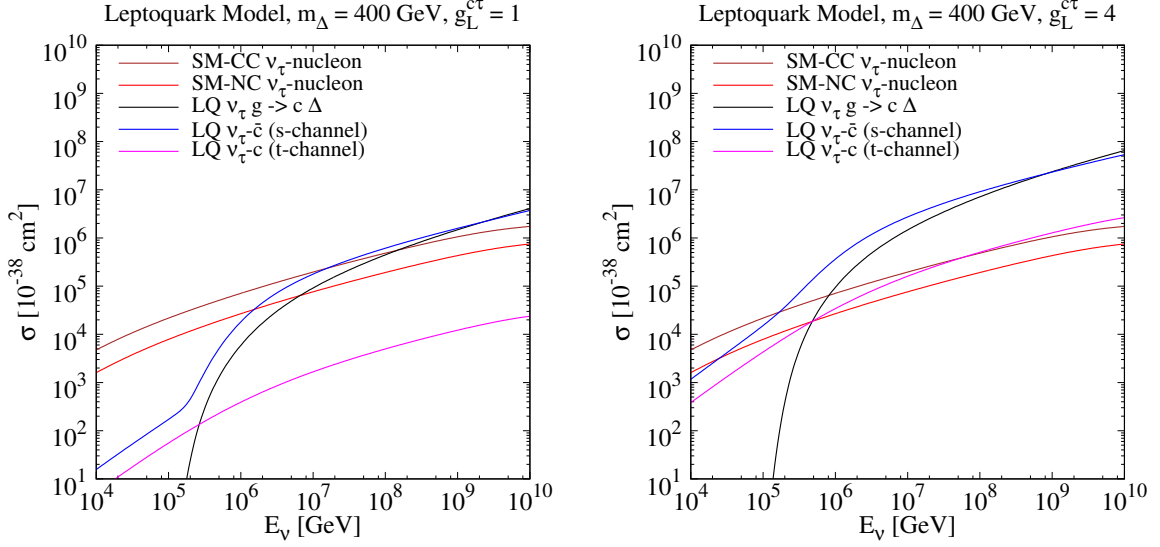


Figure 9. ν_τ -nucleon cross sections: CC contribution in the SM, NC contribution in the SM, ν_τ -gluon contribution, ν_τ -c-quark s-channel contribution, ν_τ -c-quark t-channel contribution. For the LQ cross sections $m_\Delta = 400$ GeV and $g_L^{c\tau} = 1$ (left) and $g_L^{c\tau} = 4$ (right).

of events. We see that the nonstandard effects appear only at high neutrino energies ($E_\nu \gtrsim 500$ TeV), anticipating a modest sensitivity to LQs with current IceCube data. This instigates us to investigate the situation with maximal future sensitivity of IceCube and IceCube-Gen2 [90] which we postpone to Sec. 4.

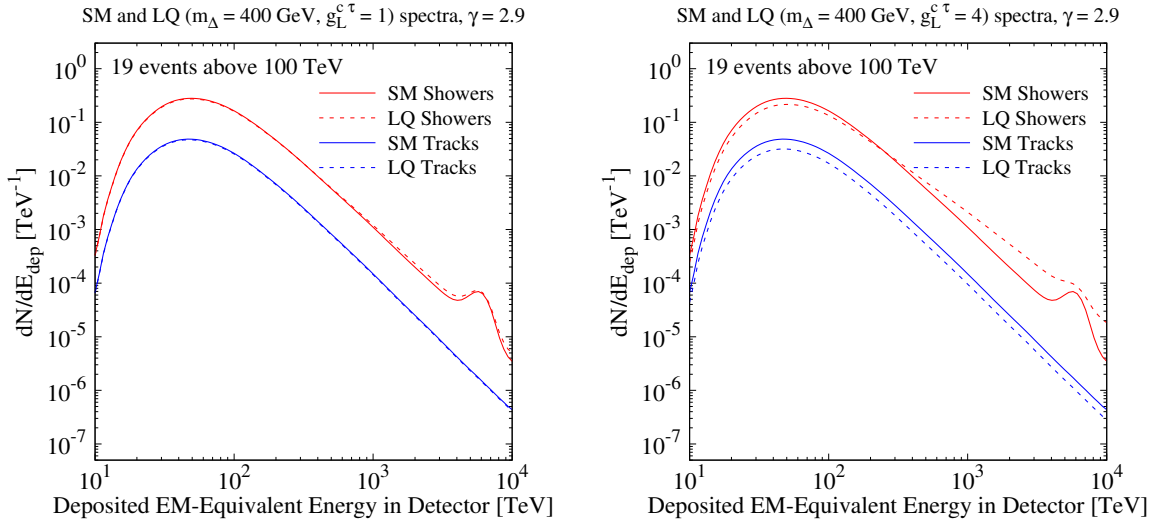


Figure 10. Comparison between the distribution of shower and track events for the SM and two representative LQ scenarios: $m_\Delta = 400$ GeV and $g_L^{c\tau} = 1$ (left panel) and $m_\Delta = 400$ GeV and $g_L^{c\tau} = 4$ (right panel). Notice that the LQ shower (and track) distributions include both the contribution of the SM as well as of the LQ interactions.

3.3 Attenuation and Regeneration Effects

The neutrinos that arrive in IceCube from the south hemisphere do not suffer Earth effects, having then an attenuation factor of $\mathcal{A}_\alpha^S(E_\nu) = \frac{1}{2}$ for an isotropic flux in Eq. (3.4). The neutrinos entering from the north hemisphere have to go through the Earth before reaching the IceCube detector with the attenuation factor of the resulting flux given by

$$\mathcal{A}_\alpha^N(E_\nu) = \frac{1}{2} \int_0^1 \mathcal{A}_\alpha(E_\nu, \theta) d \cos \theta, \quad (3.6)$$

where θ is the nadir angle, and

$$\mathcal{A}_\alpha(E_\nu, \theta) \equiv \frac{\mathcal{F}_\alpha(E_\nu, X(\theta))}{\mathcal{F}_\alpha(E_\nu, 0)}, \quad (3.7)$$

is simply a fraction of the initial flux after propagating through a column depth $X(\theta)$,

$$X(\theta) = \int_0^{L(\theta)} \rho(s) ds, \quad (3.8)$$

where $\rho(s)$ is the matter density at the point s , $L(\theta) = 2R_\oplus \cos \theta$, and R_\oplus is the Earth's radius. In the above formulas, the function \mathcal{F}_α is defined by

$$\mathcal{F}_\alpha(E, X(\theta)) \equiv \frac{\partial \Phi_\alpha}{\partial E}(E, X(\theta)). \quad (3.9)$$

To calculate $\mathcal{A}_\alpha^N(E_\nu)$ we need to solve the coupled integro-differential transport equations given in Appendix B which include absorption and regeneration effects via particle decays. We have followed the prescription described in Ref. [82] to numerically solve these equations. Furthermore, we assumed that the absorption of τ and $\Delta^{(2/3)}$ is only given by their decays into lighter particles, neglecting the subdominant scattering contributions.

The average attenuation factor $\mathcal{A}_\alpha^N(E_\nu)$ for each (anti-)neutrino flavor is shown in Fig. 11 for the SM (left panel), and for a LQ scenario with $m_\Delta = 400$ GeV and $g_L^{c\tau} = 2$ (right panel). As expected, the attenuation factors $\mathcal{A}_{\nu_\tau}^N$ ($\mathcal{A}_{\bar{\nu}_\tau}^N$) are highly affected by LQ interactions for $E_\nu \gtrsim 500$ TeV. Note, however, that since the incoming flux falls rapidly with E_ν , this effect turns out to be smaller than suggested by Fig. 11. Furthermore, we included the regeneration effects in our simulation which can lower the attenuation factors by at most 10%.

4 Statistical Data Analysis at IceCube, Present and Future

As stated in previous Sections, we use the 6-year HESE sample in the energy range [100 TeV, 10 PeV] [78]. To quantify the goodness-of-fit of each model we follow the maximum likelihood method described in Ref. [83]. The test statistic is defined by

$$-2 \ln L(H)/L_{\text{sat}} = -2 \sum_i^{N_{\text{bins}}} \ln(e^{o_i - n_i} (n_i/o_i)^{o_i}), \quad (4.1)$$

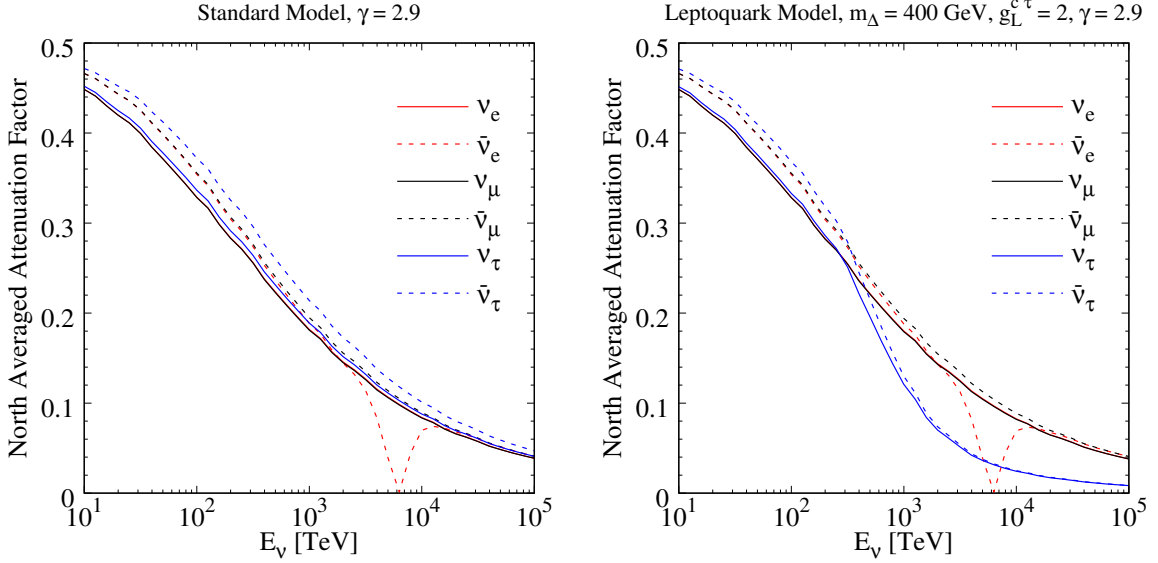


Figure 11. Average attenuation factor $\mathcal{A}_\alpha^N(E_\nu)$ for each (anti-)neutrino flavor for the SM (left panel) and for a LQ model with $m_\Delta = 400$ GeV and $g_L^{c\tau} = 2$ (right panel). These results have been obtained by fixing $\gamma = 2.9$, but they only show a mild dependence on this parameter.

where $L(H)$ is the likelihood of the tested hypothesis H (product of Poisson probabilities), and L_{sat} is the likelihood of the model that predicts the exact observed outcome, i.e. $n_i \equiv o_i$. Moreover, the values of o_i and n_i correspond to the observed and predicted number of events in the bin i , respectively. We divide the events sample in the neutrino energy range [100 TeV, 10 PeV] in 10 logarithmic energy bins for tracks and as many for showers. The total number of bins, $N_{\text{bins}} = 20$, is comparable to the 28 events detected above 100 TeV. We consider a track to shower misidentification factor (missID) of 20%, which is reasonable considering that IceCube has measured it to be approximately 30% for low energy tracks [79] and since it is expected to decrease with energy. Nevertheless, we have verified that the final results are unaffected by using a 10% or a 30% missID factor, similarly to what has been obtained in Ref. [63].

We reiterate that in our statistical analysis we consider 5 parameters:

$$\gamma, C_0, m_\Delta, g_L^{c\tau}, g_R^{b\tau}, \quad (4.2)$$

which we vary as $m_\Delta \in [300 \text{ GeV}, 700 \text{ GeV}]$, $|g_L^{c\tau}| \in [1, 4]$, and we set $g_R^{b\tau} \approx 0$ since it does not directly contribute to the cross-sections relevant to this study.

4.1 Current Data Analysis

To evaluate the quality of the fit of a hypothesis H with respect to current data, we compute the minimum of the test statistic (4.1) and its corresponding p-value, obtained by simulating pseudo-data with the best fit values of γ and C_0 . As already mentioned in the text, we find that the SM best fit point yields $\gamma = 2.98$ and $C_0 = 2.63 \text{ GeV cm}^{-2} \text{ str}^{-1} \text{ s}^{-1}$ with a test statistic value of 17.05, and a p-value of 0.25. This indicates that the SM

compatibility with the current data is quite acceptable.

The results obtained in the LQ scenario are shown in Fig. 12 for different values of LQ mass m_Δ and coupling $|g_L^{c\tau}|$. We find that the best fit point is given by $(m_\Delta, |g_L^{c\tau}|) = (500 \text{ GeV}, 2.5)$ with a minimum test statistic of 16.7, and therefore the event distribution of the SM and the best LQ model are indistinguishable from the IceCube data, also shown in left panel of Fig. 13. From the right panel of Fig. 13 we learn that only LQ models with very large $|g_L^{c\tau}| \approx 3.5$ and small masses $m_\Delta \approx 300 \text{ GeV}$ can be excluded by current IceCube data to 95% CL ($p \leq 0.05$). These parameters, however, are already excluded by the limits arising from the Z -pole observables, as discussed in Sec. 2.

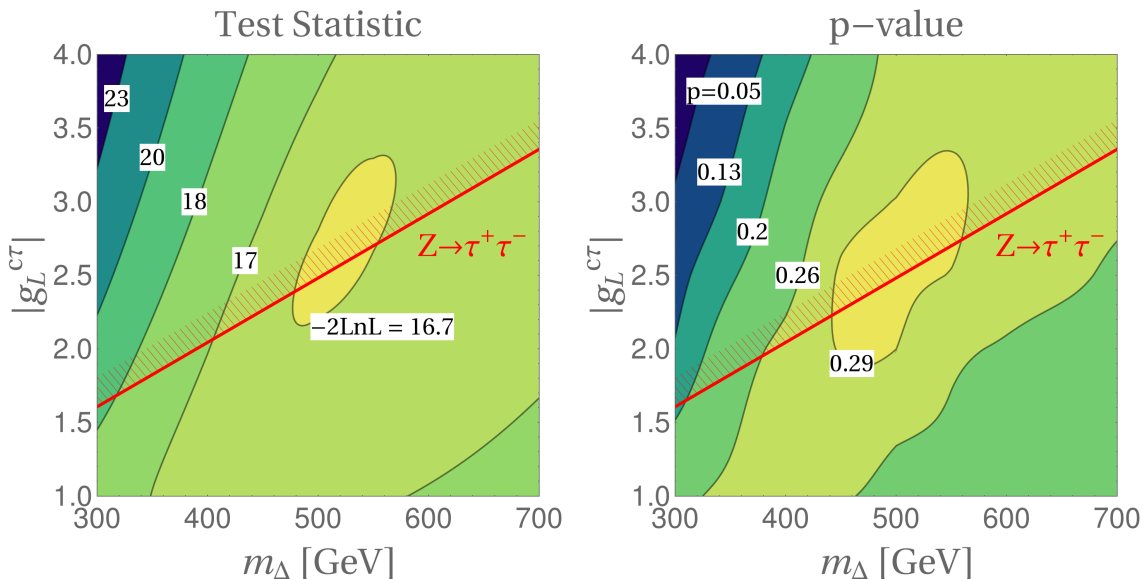


Figure 12. Summary of the best fit analysis of LQ models characterized by the values of m_Δ and $|g_{c\tau}|$. These results are based on the minimization of the test statistic defined in Eq. (4.1) with respect to γ and C_0 using the IceCube 6-year data sample. In the left panel we show contour lines for the values of the test statistic, while in the right panel we also plot contour lines but considering the obtained p-value. We show in both figures the exclusion coming from the Z -pole observables discussed in Sec. 2.2.

4.2 Future IceCube(-Gen2) Projections

To investigate the projected sensitivity of IceCube to our LQ scenario, we compute the projected exclusion regions in the plane $(m_\Delta, |g_L^{c\tau}|)$ by assuming the SM is the null hypothesis. We considered the test statistic defined by the likelihood ratio between the LQ and the SM hypotheses, given by $q = -2 \log L(\text{LQ})/L(\text{SM})$ with $L(\text{LQ})$ and $L(\text{SM})$ defined analogously to Eq. (4.1). The value of q is obtained after the minimization of each hypothesis with respect to (γ, C_0) by using projected data, which is generated from Monte Carlo simulations of the SM best fit to current data. More specifically, we evaluate the luminosity \mathcal{L} , at which the projected data is simulated, by using multiples of current 6-year exposure. To establish a criteria for exclusion we consider the p-value associated to each tested value of q . We simply assume that q follows a χ^2 -distribution with k degrees of

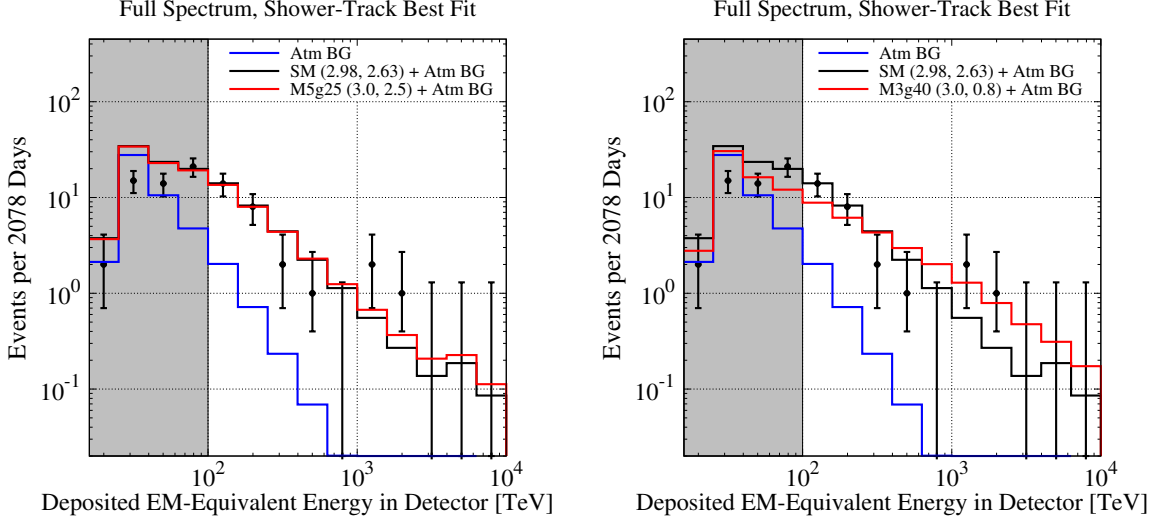


Figure 13. Comparison between the SM and LQ best fit curves to the IceCube 6-year dataset. In the left panel we show the best fit curve for $(m_\Delta, |g_L^{c\tau}|) = (500 \text{ GeV}, 2.5)$, which is one representative case of scenarios with $-2 \ln L = 16.7$. In the right panel, we show the best fit curve for $(m_\Delta, |g_L^{c\tau}|) = (300 \text{ GeV}, 4)$, which has a p-value around 0.05 and therefore it is in tension with current data. In the plot legend we quote within parentheses the best fit values of γ and C_0 for each model.

freedom, where k is the difference in the number of parameters between the LQ and SM hypotheses, which in our case is $k = 2$. Thus, for a given value of q , the p-value is given by $p = \exp(-q/2)$.

In Fig. 14 we plot our results as the projected 95% CL exclusion regions in the $(m_\Delta, |g_L^{c\tau}|)$ plane, along with the limits arising from the Z -pole observables, as well as the region eliminated by the reinterpretation of LHC searches for pair-produced LQs decaying into $b\tau$ [71, 72], $c\nu$ [75] and $t\tau$ [73, 74], c.f. discussion in Section 2. We see that the parameter region accessible to IceCube increases at a modest pace with the luminosity \mathcal{L} , reaching the corners $(m_\Delta = 300, |g_L^{c\tau}| = 1)$ and $(m_\Delta = 600, |g_L^{c\tau}| = 4)$ only with about 20 and 40 times more events than the current data. An exposure equivalent to 10 (40) times the current one might be within reach of IceCube-Gen2 [90] after about 5 (20) years of data taking. From that plot we also see that the region of parameters accessible to IceCube(-Gen2) is already disfavored by a combination of constraints arising from the direct (LHC) and indirect searches (flavor physics and LEP).

5 Conclusions

Several authors have inquired about the potential of IceCube detector in the South Pole to search for LQs [57–63]. In most of these works LQs couple to the first generation of quarks. On the one hand this allows LQ production to profit from the valence quark contribution to the neutrino-nucleon cross section. On the other hand limits from direct searches, atomic parity violation and flavor physics are at odds with these possibilities.

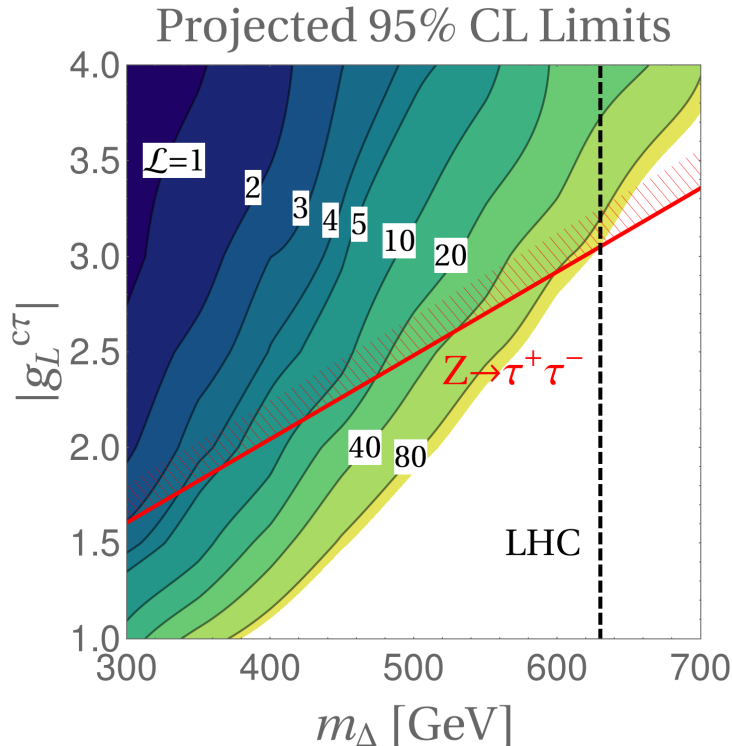


Figure 14. Estimation of the 95% CL exclusion regions in the parameter space $(m_\Delta, |g_L^{e\tau}|)$ considering several projections of IceCube data at exposures measured in units of the current 6-year data sample. We also show the constraints on large LQ couplings derived from the Z -pole observables (red line) and the lower limits on the LQ mass stemming from the reinterpretation of LHC limits on pair-produced LQs (dashed line), see Sec. 2.2 for details.

Here, instead, we focus on LQs that couple to heavy quark flavors, a scenario that recently became of particular interest in connection with B -meson semileptonic decays. The hope that IceCube could contribute to the search of this type of LQ models springs from a few considerations. First, these models cannot be dismissed by current direct or indirect detection searches. Second, their production cross section has been underestimated in the literature as the neutrino-gluon contribution has been neglected up to now. Third, attenuation effects when crossing the Earth are modified by the new LQ interactions which was not considered previously. Finally, the proposal of IceCube-Gen2 [90] allows for exploring a much higher statistics of HESE than at the present time.

In this paper we focused on a simple LQ scenario that can explain $R_{D^{(*)}}^{\text{exp}} > R_{D^{(*)}}^{\text{SM}}$ and involves only three new parameters: the LQ mass (m_Δ) and two couplings ($g_L^{e\tau}$ and $g_R^{b\tau}$). Parameter space is constrained in such a way as to solve $R_{D^{(*)}}$ and satisfy experimental constraints coming from the Z -decay modes. With parameters constrained in this way we estimate the present (future) sensitivity of IceCube (IceCube-Gen2) to this model. Our results are summarized in Fig. 14 from which we see that the parameter space accessible to IceCube/IceCube-Gen2 is already excluded by the direct searches (see Fig. 4) and the low-

energy flavor physics observables. That conclusion is based on our current understanding of the HESE data and the value of the spectral index γ in particular. If that value turns out to be lower, then also Fig. 14 would change because there would be more data corresponding to heavier LQs but with the mass still lower than about 650 GeV, to comply with the results of the direct searches at LHC.

We should also stress that in our calculation we consistently used a democratic flavor distribution of the incoming flux, which is plausible and compatible with the current data. Other possibilities are, however, possible too which is one reason more why settling that issue is of major importance for searching the effects of physics beyond the SM [78].

Acknowledgments

This work was partially supported by Fundação de Amparo à Pesquisa do Estado de São Paulo (FAPESP) and Conselho Nacional de Ciência e Tecnologia (CNPq). R.Z.F. is grateful for the hospitality of the Laboratoire de Physique Théorique of Université Paris-Sud during the final part of this work and acknowledges the CNRS for support during this time. D.B. acknowledges the INP-CNRS support via “*Inphyniti*”. This project has also received support from the European Union’s Horizon 2020 research and innovation programme under the Marie Skłodowska-Curie grant agreement N° 690575 and 674896.

A Leptoquark Contributions to the Neutrino-Nucleon Scattering Cross Section

For completeness we give here the expressions for the neutrino-nucleon scattering cross section at the parton level. The total differential cross section induced by LQs can be written as

$$\begin{aligned} \frac{d\sigma_{\nu\tau}^{\Delta}}{dy}(y, E_{\nu}) &= \int_{x_{\min}}^1 dx g(x, \hat{s}) \frac{\partial^2 \sigma^{g\nu\tau}}{\partial x \partial y}(E_{\nu}, x, y) \\ &+ \sum_q \int_0^1 dx q(x, \hat{s}) \frac{\partial^2 \sigma^{q\nu\tau}}{\partial x \partial y}(E_{\nu}, x, y), \end{aligned} \quad (\text{A.1})$$

for an incident neutrino ν_{τ} . Here $g(x, \hat{s})$ ($q(x, \hat{s})$) is the gluon (quark q) PDF of the nucleon. In our computations, we considered the NNPDF2.3 PDF sets [85], which are implemented in LHAPDF6 [86].

A.1 ν_{ℓ} -gluon contribution

We give here the expressions for the gluon-neutrino differential cross sections induced by LQs. The kinematics of these processes can be described by the following variables

$$y = \frac{E_{\nu} - E_{\Delta}}{E_{\nu}}, \quad x = \frac{Q^2}{2m_N E_{\nu} y}, \quad \hat{s} = 2x m_N E_{\nu},$$

with the inelasticity y and the Bjorken variable x defined in the intervals ⁵

$$y \in \left[\frac{\hat{s} - m_q^2 - m_{\Delta}^2 - \lambda^{1/2}(\sqrt{\hat{s}}, m_{\Delta}, m_q)}{2\hat{s}}, \frac{\hat{s} - m_q^2 - m_{\Delta}^2 + \lambda^{1/2}(\sqrt{\hat{s}}, m_{\Delta}, m_q)}{2\hat{s}} \right],$$

and

$$x \in \left[\frac{(m_q + m_{\Delta})^2}{2m_N E_{\nu}}, 1 \right],$$

where E_{ν} and E_{Δ} are the (anti-)neutrino and LQ energies in the laboratory frame, $Q^2 = -t$ is the invariant squared momentum transferred in the t -channel, m_q is the mass of the quark in the process, m_{Δ} the LQ mass, and $m_N = (m_p + m_n)/2$ is the average mass of the nucleon. We have used the fact that water is a isoscalar target, so that $N = Z$. We also define the function $\lambda(a, b, c) \equiv (a^2 - (b - c)^2)(a^2 - (b + c)^2)$.

The two diagrams that contribute to the amplitudes that enter these cross sections can be seen in Fig. 8. The cross section for $\nu_{\ell} g \rightarrow q_u \Delta^{(-2/3)}$ is given by ⁶

⁵We define $t = (p_{\nu} - p_{\Delta})^2$, where p_{ν} is the incident neutrino momentum and p_{Δ} is the LQ momentum.

⁶The cross section for the CP conjugated mode $\bar{\nu}_{\ell} g \rightarrow \bar{q}_u \Delta^{(2/3)}$ coincides with this expression.

$$\frac{\partial^2 \sigma^{g\nu_\ell}}{\partial x \partial y} = (2m_p E_\nu x) \frac{\alpha_s |g_L^{qu\ell}|^2}{8\hat{s}} \left\{ \frac{\hat{s}Q^2 + m_q^2[2(m_\Delta^2 + Q^2) + \hat{s}]}{(m_q^2 + Q^2)^2} \right. \quad (\text{A.2})$$

$$+ \frac{(Q^2 + m_\Delta^2 - \hat{s})(2m_\Delta^2 + Q^2 - \hat{s} + m_q^2)}{(m_q^2 + Q^2 - \hat{s})^2}$$

$$\left. + \frac{(\hat{s} - Q^2 - m_\Delta^2)(2m_\Delta^2 + Q^2) + m_q^2[\hat{s} - 3(Q^2 + m_\Delta^2)]}{(m_q^2 + Q^2)(m_q^2 + Q^2 - \hat{s})} \right\},$$

where N_c is the number of colors q_u and ℓ are a generic up-type quark and lepton, and $\alpha_s = \alpha_s(\hat{s})$ is the strong coupling constant at the relevant scale of the process.

A.2 ν_ℓ -quark contribution

The LQ state contributes to the neutrino-quark cross-section via an exchange of a LQ in the t -channel as depicted in Fig. 7. The SM cross-section amended with the LQ contribution reads

$$\frac{\partial^2 \sigma^{\nu_\ell q_u \rightarrow \nu_{\ell'} q_{u'}}}{\partial x \partial y} = \frac{2m_p E_\nu x}{32\pi \hat{s}^2} \left\{ \frac{\hat{u}^2 |g_L^{qu\ell'}|^2 |g_L^{q_{u'}\ell}|^2}{(\hat{u} - m_\Delta^2)^2} \right. \quad (\text{A.3})$$

$$+ \delta_{\ell\ell'} \delta_{\hat{u}u'} \left[|g_L^{u\ell}|^2 \frac{16\sqrt{2}G_f m_Z^2 u^2 (g_A^u - g_V^u)}{(\hat{u} - m_\Delta^2)(\hat{t} - m_Z^2)} \right.$$

$$\left. + \frac{8G_F^2 m_Z^4 \left[(\hat{s}^2 + \hat{u}^2) \left((g_A^u)^2 + (g_V^u)^2 \right) + 2g_A^u g_V^u (\hat{s}^2 - \hat{u}^2) \right]}{(\hat{t} - m_Z^2)^2} \right] \left. \right\},$$

where $q_u, q_{u'}$ are generic up-type quarks and ℓ, ℓ' are generic leptons. We define the weak couplings $g_V^u = T_u^3 - 2Q_u \sin^2 \theta_W = 1/2 - 4/3 \sin^2 \theta_W$ and $g_A^u = T_u^3 = 1/2$. The Mandelstam variables in our setup are taken to be

$$\hat{s} = (p_{\nu_\ell} + p_{q_u})^2, \quad \hat{t} = (p_{\nu_\ell} - p_{\nu_{\ell'}})^2 \quad \text{and} \quad \hat{u} = (p_{\nu_\ell} - p_{q_{u'}})^2. \quad (\text{A.4})$$

Similarly, the $\nu\bar{q}$ cross-section receives a s -channel contribution from the LQ state, as shown in Fig. 7. The corresponding expression is given by

$$\begin{aligned}
\frac{\partial^2 \sigma^{\nu_\ell \bar{q}_u \rightarrow \nu_{\ell'} \bar{q}_{u'}}}{\partial x \partial y} &= \frac{2m_p E_\nu x}{32\pi \hat{s}^2} \left\{ \frac{\hat{u}^2 |g_L^{qu\ell'}|^2 |g_L^{qu\ell}|^2}{(\hat{s} - m_\Delta^2)^2 + m_\Delta^2 \Gamma_\Delta^2} \right. \\
&+ \delta_{\ell\ell'} \delta_{uu'} \left[|g_L^{u\ell}|^2 \frac{16\sqrt{2} G_f m_Z^2 \hat{u}^2 (g_A^u - g_V^u)(\hat{s} - m_\Delta^2)}{((\hat{s} - m_\Delta^2)^2 + m_\Delta^2 \Gamma_\Delta^2)(\hat{t} - m_Z^2)} \right. \\
&\left. \left. + \frac{8G_F^2 m_Z^4 \left[(\hat{s}^2 + \hat{u}^2) \left((g_A^u)^2 + (g_V^u)^2 \right) + 2g_A^u g_V^u (\hat{s}^2 - \hat{u}^2) \right]}{(\hat{t} - m_Z^2)^2} \right] \right\}. \tag{A.5}
\end{aligned}$$

where Γ_Δ is the total LQ decay width.

B Transport Equations Including the Leptoquark Contribution

The set of transport equations that have to be solved in order to compute the attenuation factor for the neutrino flux is the following

$$\begin{aligned}
\frac{\partial \mathcal{F}_{\nu_\ell}}{\partial X} &= -N_A [\sigma_{\nu_\ell N}^{\text{CC}}(E) + \sigma_{\nu_\ell N}^{\text{NC}}(E) + \sigma_{\nu_\ell}^\Delta(E)] \mathcal{F}_{\nu_\ell}(E, X) \\
&+ \frac{1}{c\rho(X)} \int_0^1 \frac{1}{1-y} \left[\frac{d\Gamma_{\tau \rightarrow \nu_\ell X'}}{dy}(E_y, y) \mathcal{F}_\tau(E_y, X) + \frac{d\Gamma_{\Delta \rightarrow \nu_\ell X'}}{dy}(E_y, y) \mathcal{F}_\Delta(E_y, X) \right] \\
&+ N_A \int_0^1 \frac{dy}{1-y} \left[\frac{d\sigma_{\nu_\ell N}^{\text{NC}}(E_y, y)}{dy} \mathcal{F}_{\nu_\ell}(E_y, X) + \frac{d\sigma_{\nu_m \rightarrow \nu_\ell}^{\Delta-q}(E_y, y)}{dy} \mathcal{F}_{\nu_m}(E_y, X) \right], \tag{B.1}
\end{aligned}$$

$$\frac{\partial \mathcal{F}_\tau}{\partial X} = -\frac{m_\tau}{E\tau_\tau c\rho(X)} \mathcal{F}_\tau(E, X) + N_A \int_0^1 \frac{dy}{1-y} \frac{d\sigma_{\nu_\tau N}^{\text{CC}}(E_y, y)}{dy} \mathcal{F}_{\nu_\tau}(E_y, X), \tag{B.2}$$

$$\frac{\partial \mathcal{F}_\Delta}{\partial X} = -\frac{m_\Delta}{E\tau_\Delta c\rho(X)} \mathcal{F}_\Delta(E, X) + N_A \int_0^1 \frac{dy}{1-y} \frac{d\sigma_{\nu_\beta N}^{\Delta-g}(E_y, y)}{dy} \mathcal{F}_{\nu_\beta}(E_y, X), \tag{B.3}$$

where $E_y = E/(1-y)$, m_τ (m_Δ) is the τ (Δ) mass, τ_τ (τ_Δ) is the τ (Δ) lifetime, $\sigma_{\nu_\ell}^\Delta$ is the total LQ contribution to the neutrino-nucleon cross section, $d\sigma_{\nu_\ell}^{\Delta-q}/dy$ ($d\sigma_{\nu_\ell}^{\Delta-g}/dy$) is the neutrino-quark (neutrino-gluon) part of the differential cross section and $\sigma_{\nu_\ell N}^{\text{CC,NC}}$ are the SM CC and NC neutrino-nucleon cross sections. The distribution of the τ partial decay widths $d\Gamma_{\tau \rightarrow \nu_\ell X'}/dy$ can be found in Ref. [82, 87] while the distribution of the Δ partial decay width $d\Gamma_{\Delta \rightarrow \nu_\ell X'}/dy$ is given by

$$\frac{d\Gamma_{\Delta \rightarrow \nu_\ell X'}}{dy} = \Gamma_\Delta \frac{(1-y)}{\sqrt{\gamma^2 - 1}} \gamma \left[\Theta \left[\left(\frac{1}{2} + \frac{\sqrt{\gamma^2 - 1}}{2\gamma} \right) - y \right] - \Theta \left[\left(\frac{1}{2} - \frac{\sqrt{\gamma^2 - 1}}{2\gamma} \right) - y \right] \right] \tag{B.4}$$

where $\gamma = E_\Delta/m_\Delta$, $\Theta(x)$ is the Heavyside function.

C $B \rightarrow D\ell\bar{\nu}$ expressions

The contribution of the effective Hamiltonian 2.3 to $\mathcal{B}(B \rightarrow D\ell\nu)$ is given by

$$\begin{aligned} \frac{d\Gamma}{dq^2}(B \rightarrow D\ell\nu) = & \frac{G_F^2 |V_{cb}|^2}{192\pi^3 m_B^3} |f_+(q^2)|^2 \left\{ c_+^\ell(q^2) + |g_T(\mu)|^2 c_T^\ell(q^2) \left| \frac{f_T(q^2)}{f_+(q^2)} \right|^2 \right. \\ & + c_{TV}^\ell(q^2) \operatorname{Re}[g_T^*(\mu)] \frac{f_T(q^2, \mu)}{f_+(q^2)} \\ & \left. + c_0^\ell(q^2) \left| 1 + g_S(\mu) \frac{q^2}{m_\ell(m_b(\mu) - m_c(\mu))} \right|^2 \left| \frac{f_0(q^2)}{f_+(q^2)} \right|^2 \right\}, \end{aligned} \quad (\text{C.1})$$

where $f_{0,+T}(q^2)$ are the $B \rightarrow D$ form factors as defined in Ref. [88]. The expressions for the phase-space functions $c_i^\ell(q^2)$ read [88, 89]

$$c_+^\ell(q^2) = \lambda^{3/2}(\sqrt{q^2}, m_B, m_D) \left[1 - \frac{3}{2} \frac{m_\ell^2}{q^2} + \frac{1}{2} \left(\frac{m_\ell^2}{q^2} \right)^3 \right], \quad (\text{C.2})$$

$$c_0^\ell(q^2) = m_\ell^2 \lambda^{1/2}(\sqrt{q^2}, m_B, m_D) \frac{3}{2} \frac{m_B^4}{q^2} \left(1 - \frac{m_\ell^2}{q^2} \right)^2 \left(1 - \frac{m_D^2}{m_B^2} \right)^2, \quad (\text{C.3})$$

$$c_T^\ell(q^2) = \lambda^{3/2}(\sqrt{q^2}, m_B, m_D) \frac{2q^2}{(m_B + m_D)^2} \left[1 - 3 \left(\frac{m_\ell^2}{q^2} \right)^2 + 2 \left(\frac{m_\ell^2}{q^2} \right)^3 \right], \quad (\text{C.4})$$

$$c_{TV}^\ell(q^2) = \frac{6m_\ell}{m_B + m_D} \lambda^{3/2}(\sqrt{q^2}, m_B, m_D) \left(1 - \frac{m_\ell^2}{q^2} \right)^2. \quad (\text{C.5})$$

The expressions for $\mathcal{B}(B \rightarrow D^*\ell\bar{\nu})$ can be found in Ref. [67], which we have independently checked.

References

- [1] H. Georgi and S. L. Glashow, Phys. Rev. Lett. **32**, 438 (1974).
- [2] J. C. Pati and A. Salam, Phys. Rev. D **10**, 275 (1974) Erratum: [Phys. Rev. D **11**, 703 (1975)].
- [3] L. F. Abbott and E. Farhi, Phys. Lett. **101B**, 69 (1981).
- [4] B. Schrempp and F. Schrempp, Phys. Lett. **153B**, 101 (1985).
- [5] J. Wudka, Phys. Lett. **167B**, 337 (1986).
- [6] W. Buchmuller, R. Ruckl and D. Wyler, Phys. Lett. B **191**, 442 (1987) Erratum: [Phys. Lett. B **448**, 320 (1999)].
- [7] I. Doršner, S. Fajfer, A. Greljo, J. F. Kamenik and N. Košnik, Phys. Rept. **641**, 1 (2016) [arXiv:1603.04993 [hep-ph]].
- [8] A. Aktas *et al.* [H1 Collaboration], Phys. Lett. B **629**, 9 (2005) [hep-ex/0506044].
- [9] B. Diaz, M. Schmaltz and Y. M. Zhong, JHEP **1710**, 097 (2017) [arXiv:1706.05033 [hep-ph]].

- [10] A. Greljo and D. Marzocca, *Eur. Phys. J. C* **77** (2017) no.8, 548 [arXiv:1704.09015 [hep-ph]].
- [11] R. Aaij *et al.* [LHCb Collaboration], *Phys. Rev. Lett.* **113**, 151601 (2014) [arXiv:1406.6482 [hep-ex]].
- [12] R. Aaij *et al.* [LHCb Collaboration], *JHEP* **1708**, 055 (2017) [arXiv:1705.05802 [hep-ex]].
- [13] G. Hiller and F. Kruger, *Phys. Rev. D* **69**, 074020 (2004) [hep-ph/0310219].
- [14] M. Bordone, G. Isidori and A. Pattori, *Eur. Phys. J. C* **76**, no. 8, 440 (2016) [arXiv:1605.07633 [hep-ph]].
- [15] Y. Amhis *et al.* [HFLAV Collaboration], *Eur. Phys. J. C* **77**, no. 12, 895 (2017) [arXiv:1612.07233 [hep-ex]].
- [16] J. P. Lees *et al.* [BaBar Collaboration], *Phys. Rev. Lett.* **109**, 101802 (2012) [arXiv:1205.5442 [hep-ex]].
- [17] M. Huschle *et al.* [Belle Collaboration], *Phys. Rev. D* **92**, no. 7, 072014 (2015) [arXiv:1507.03233 [hep-ex]].
- [18] Y. Sato *et al.* [Belle Collaboration], *Phys. Rev. D* **94**, no. 7, 072007 (2016) [arXiv:1607.07923 [hep-ex]].
- [19] R. Aaij *et al.* [LHCb Collaboration], *Phys. Rev. Lett.* **115**, no. 11, 111803 (2015) Erratum: [*Phys. Rev. Lett.* **115**, no. 15, 159901 (2015)] [arXiv:1506.08614 [hep-ex]].
- [20] S. Hirose *et al.* [Belle Collaboration], *Phys. Rev. Lett.* **118**, no. 21, 211801 (2017) [arXiv:1612.00529 [hep-ex]].
- [21] H. Na *et al.* [HPQCD Collaboration], *Phys. Rev. D* **92**, no. 5, 054510 (2015) Erratum: [*Phys. Rev. D* **93**, no. 11, 119906 (2016)] [arXiv:1505.03925 [hep-lat]].
- [22] J. A. Bailey *et al.* [MILC Collaboration], *Phys. Rev. D* **92**, no. 3, 034506 (2015) [arXiv:1503.07237 [hep-lat]].
- [23] R. Aaij *et al.* [LHCb Collaboration], arXiv:1711.02505 [hep-ex].
- [24] S. Fajfer, J. F. Kamenik and I. Nisandzic, *Phys. Rev. D* **85**, 094025 (2012) [arXiv:1203.2654 [hep-ph]].
- [25] D. Bigi, P. Gambino and S. Schacht, *JHEP* **1711** (2017) 061 [arXiv:1707.09509 [hep-ph]].
- [26] R. Aaij *et al.* [LHCb Collaboration], arXiv:1711.05623 [hep-ex].
- [27] G. Hiller and M. Schmaltz, *Phys. Rev. D* **90**, 054014 (2014) [arXiv:1408.1627 [hep-ph]].
- [28] D. Ghosh, M. Nardecchia and S. A. Renner, *JHEP* **1412**, 131 (2014) [arXiv:1408.4097 [hep-ph]].
- [29] R. Alonso, B. Grinstein and J. Martin Camalich, *JHEP* **1510**, 184 (2015) [arXiv:1505.05164 [hep-ph]].
- [30] S. Fajfer and N. Košnik, *Phys. Lett. B* **755**, 270 (2016) [arXiv:1511.06024 [hep-ph]].
- [31] R. Barbieri, G. Isidori, A. Pattori and F. Senia, *Eur. Phys. J. C* **76**, no. 2, 67 (2016) [arXiv:1512.01560 [hep-ph]].
- [32] M. Bauer and M. Neubert, *Phys. Rev. Lett.* **116**, no. 14, 141802 (2016) [arXiv:1511.01900 [hep-ph]].
- [33] F. F. Deppisch, S. Kulkarni, H. Päs and E. Schumacher, *Phys. Rev. D* **94**, no. 1, 013003

- (2016) [arXiv:1603.07672 [hep-ph]].
- [34] P. Arnan, L. Hofer, F. Mescia and A. Crivellin, JHEP **1704**, 043 (2017) [arXiv:1608.07832 [hep-ph]].
 - [35] D. Bečirević, S. Fajfer, N. Košnik and O. Sumensari, Phys. Rev. D **94**, no. 11, 115021 (2016) [arXiv:1608.08501 [hep-ph]].
 - [36] P. Cox, A. Kusenko, O. Sumensari and T. T. Yanagida, JHEP **1703** (2017) 035 [arXiv:1612.03923 [hep-ph]].
 - [37] G. Hiller, D. Loose and K. Schönwald, JHEP **1612**, 027 (2016) [arXiv:1609.08895 [hep-ph]].
 - [38] I. Doršner, S. Fajfer, D. A. Faroughy and N. Košnik, JHEP **1710**, 188 (2017) [arXiv:1706.07779 [hep-ph]].
 - [39] R. Barbieri, C. W. Murphy and F. Senia, Eur. Phys. J. C **77**, no. 1, 8 (2017) [arXiv:1611.04930 [hep-ph]].
 - [40] D. Bečirević and O. Sumensari, JHEP **1708**, 104 (2017) [arXiv:1704.05835 [hep-ph]].
 - [41] S. Fajfer, N. Košnik and L. Vale Silva, arXiv:1802.00786 [hep-ph].
 - [42] Y. Cai, J. Gargalionis, M. A. Schmidt and R. R. Volkas, JHEP **1710**, 047 (2017) [arXiv:1704.05849 [hep-ph]].
 - [43] D. Aloni, A. Dery, C. Frugiuele and Y. Nir, JHEP **1711** (2017) 109 [arXiv:1708.06161 [hep-ph]].
 - [44] A. Crivellin, D. Müller, A. Signer and Y. Ulrich, Phys. Rev. D **97** (2018) no.1, 015019 [arXiv:1706.08511 [hep-ph]].
 - [45] A. Crivellin, D. Müller and T. Ota, JHEP **1709**, 040 (2017) [arXiv:1703.09226 [hep-ph]].
 - [46] D. Buttazzo, A. Greljo, G. Isidori and D. Marzocca, JHEP **1711**, 044 (2017) [arXiv:1706.07808 [hep-ph]].
 - [47] L. Di Luzio, A. Greljo and M. Nardecchia, Phys. Rev. D **96**, no. 11, 115011 (2017) [arXiv:1708.08450 [hep-ph]].
 - [48] L. Calibbi, A. Crivellin and T. Li, arXiv:1709.00692 [hep-ph].
 - [49] M. Bordone, C. Cornella, J. Fuentes-Martin and G. Isidori, arXiv:1712.01368 [hep-ph].
 - [50] R. Barbieri and A. Tesi, arXiv:1712.06844 [hep-ph].
 - [51] L. Di Luzio, M. Kirk and A. Lenz, arXiv:1712.06572 [hep-ph].
 - [52] J. M. Cline, Phys. Rev. D **97**, no. 1, 015013 (2018) doi:10.1103/PhysRevD.97.015013 [arXiv:1710.02140 [hep-ph]].
 - [53] M. Blanke and A. Crivellin, arXiv:1801.07256 [hep-ph].
 - [54] N. Assad, B. Fornal and B. Grinstein, Phys. Lett. B **777**, 324 (2018) doi:10.1016/j.physletb.2017.12.042 [arXiv:1708.06350 [hep-ph]].
 - [55] W. Altmannshofer, P. S. Bhupal Dev and A. Soni, Phys. Rev. D **96**, no. 9, 095010 (2017) doi:10.1103/PhysRevD.96.095010 [arXiv:1704.06659 [hep-ph]].
 - [56] M. G. Aartsen *et al.* [IceCube Collaboration], Science **342**, 1242856 (2013) [arXiv:1311.5238 [astro-ph.HE]].
 - [57] L. A. Anchordoqui, C. A. Garcia Canal, H. Goldberg, D. Gomez Dumm and F. Halzen,

- Phys. Rev. D **74**, 125021 (2006) [hep-ph/0609214].
- [58] V. Barger and W. Y. Keung, Phys. Lett. B **727**, 190 (2013) [arXiv:1305.6907 [hep-ph]].
- [59] B. Dutta, Y. Gao, T. Li, C. Rott and L. E. Strigari, Phys. Rev. D **91**, 125015 (2015) [arXiv:1505.00028 [hep-ph]].
- [60] N. Mileo, A. de la Puente and A. Szyrkman, JHEP **1611**, 124 (2016) [arXiv:1608.02529 [hep-ph]].
- [61] U. K. Dey and S. Mohanty, JHEP **1604**, 187 (2016) [arXiv:1505.01037 [hep-ph]].
- [62] B. Chauhan, B. Kindra and A. Narang, arXiv:1706.04598 [hep-ph].
- [63] U. K. Dey, D. Kar, M. Mitra, M. Spannowsky and A. C. Vincent, arXiv:1709.02009 [hep-ph].
- [64] P. S. B. Dev, D. K. Ghosh and W. Rodejohann, Phys. Lett. B **762** (2016) 116 doi:10.1016/j.physletb.2016.08.066 [arXiv:1605.09743 [hep-ph]].
- [65] M. González-Alonso, J. Martin Camalich and K. Mimouni, Phys. Lett. B **772** (2017) 777 [arXiv:1706.00410 [hep-ph]].
- [66] F. U. Bernlochner, Z. Ligeti, M. Papucci and D. J. Robinson, Phys. Rev. D **95**, no. 11, 115008 (2017) [arXiv:1703.05330 [hep-ph]].
- [67] Y. Sakaki, M. Tanaka, A. Tayduganov and R. Watanabe, Phys. Rev. D **88**, no. 9, 094012 (2013) [arXiv:1309.0301 [hep-ph]].
- [68] M. Bona *et al.* [UTfit Collaboration], JHEP **0610**, 081 (2006) [hep-ph/0606167].
- [69] C. Patrignani *et al.* [Particle Data Group], Chin. Phys. C **40**, no. 10, 100001 (2016).
- [70] S. Schael *et al.* [ALEPH and DELPHI and L3 and OPAL and SLD Collaborations and LEP Electroweak Working Group and SLD Electroweak Group and SLD Heavy Flavour Group], Phys. Rept. **427**, 257 (2006) [hep-ex/0509008].
- [71] V. Khachatryan *et al.* [CMS Collaboration], JHEP **1703** (2017) 077 [arXiv:1612.01190 [hep-ex]].
- [72] CMS Collaboration [CMS Collaboration], CMS-PAS-EXO-16-023.
- [73] V. Khachatryan *et al.* [CMS Collaboration], JHEP **1507**, 042 (2015) Erratum: [JHEP **1611**, 056 (2016)] [arXiv:1503.09049 [hep-ex]].
- [74] A. M. Sirunyan *et al.* [CMS Collaboration], arXiv:1803.02864 [hep-ex].
- [75] CMS Collaboration [CMS Collaboration], CMS-PAS-SUS-18-001.
- [76] M. G. Aartsen *et al.* [IceCube Collaboration], Phys. Rev. Lett. **113**, 101101 (2014) [arXiv:1405.5303 [astro-ph.HE]].
- [77] M. G. Aartsen *et al.* [IceCube Collaboration], arXiv:1510.05223 [astro-ph.HE].
- [78] M. G. Aartsen *et al.* [IceCube Collaboration], arXiv:1710.01191 [astro-ph.HE].
- [79] M. G. Aartsen *et al.* [IceCube Collaboration], Phys. Rev. Lett. **114**, no. 17, 171102 (2015) [arXiv:1502.03376 [astro-ph.HE]].
- [80] H. Nunokawa, B. Panes and R. Zukanovich Funchal, JCAP **1610**, no. 10, 036 (2016) [arXiv:1604.08595 [hep-ph]].
- [81] S. Palomares-Ruiz, A. C. Vincent and O. Mena, Phys. Rev. D **91**, no. 10, 103008 (2015) [arXiv:1502.02649 [astro-ph.HE]].

- [82] S. Rakshit and E. Reya, Phys. Rev. D **74**, 103006 (2006) [hep-ph/0608054].
- [83] M. G. Aartsen *et al.* [IceCube Collaboration], Astrophys. J. **809**, no. 1, 98 (2015) [arXiv:1507.03991 [astro-ph.HE]].
- [84] D. Xu [IceCube Collaboration], PoS ICHEP **2016**, 452 (2016) [arXiv:1702.05238 [astro-ph.HE]].
- [85] R. D. Ball *et al.*, Nucl. Phys. B **867**, 244 (2013) [arXiv:1207.1303 [hep-ph]].
- [86] A. Buckley, J. Ferrando, S. Lloyd, K. Nordström, B. Page, M. Rüfenacht, M. Schönherr and G. Watt, Eur. Phys. J. C **75**, 132 (2015) [arXiv:1412.7420 [hep-ph]].
- [87] S. I. Dutta, M. H. Reno and I. Sarcevic, Phys. Rev. D **62**, 123001 (2000) [hep-ph/0005310].
- [88] D. Bečirević, N. Košnik, O. Sumensari and R. Zukanovich Funchal, JHEP **1611**, 035 (2016) [arXiv:1608.07583 [hep-ph]].
- [89] D. Bečirević, N. Košnik and A. Tayduganov, Phys. Lett. B **716**, 208 (2012) [arXiv:1206.4977 [hep-ph]].
- [90] M. G. Aartsen *et al.* [IceCube Collaboration], arXiv:1510.05228 [astro-ph.IM].
- [91] A. C. Vincent, S. Palomares-Ruiz and O. Mena, Phys. Rev. D **94**, no. 2, 023009 (2016) doi:10.1103/PhysRevD.94.023009 [arXiv:1605.01556 [astro-ph.HE]].